Ligand-based rational design, synthesis and evaluation of novel potential chemical chaperones for opsin

Gaia Pasqualetto [1], Elisa Pileggi [1], Martin Schepelmann [2,3], Carmine Varricchio [1], Malgorzata Rozanowska [3,4], Andrea Brancale [1], and Marcella Bassetto [5,*

[1]   School of Pharmacy and Pharmaceutical Sciences, Cardiff University, Cardiff CF10 3NB, UK
[2]   Institute of Pathophysiology and Allergy Research, Medical University of Vienna, Vienna 1090, Austria
[3]   School of Optometry and Vision Sciences, Cardiff University, Cardiff CF24 4HQ, UK
[4]   Cardiff Institute for Tissue Engineering and Repair (CITER), Cardiff University, Cardiff CF10 3NB, UK
[5]   Department of Chemistry, College of Science and Engineering, Swansea University, Swansea SA2 8PP, UK
*   Correspondence: M.B., marcella.bassetto@swansea.ac.uk.

Abstract: Inherited blinding diseases retinitis pigmentosa (RP) and a subset of Leber's congenital amaurosis (LCA) are caused by the misfolding and mistrafficking of rhodopsin molecules, which aggregate and accumulate in the endoplasmic reticulum (ER), leading to photoreceptor cell death. One potential therapeutic strategy to prevent the loss of photoreceptors in these conditions is to identify opsin-binding compounds that act as chemical chaperones for opsin, aiding its proper folding and trafficking to the outer cell membrane. Aiming to identify novel compounds with such effect, a rational ligand-based approach was applied to the structure of the visual pigment chromophore, 11-*cis*-retinal, and its locked analogue 11-*cis*-6mr-retinal. Following molecular docking studies on the main chromophore binding site of rhodopsin, 49 novel compounds were synthesized according to optimized one- to seven-step synthetic routes. These agents were evaluated for their ability to compete for the chromophore binding site of opsin, and their capacity to increase the trafficking of the P23H opsin mutant from the ER to the cell membrane. Different new molecules displayed an effect in at least one assay, acting either as chemical chaperones or as stabilizers of the 9-cis-retinal-rhodopsin complex. These compounds could provide the basis to develop novel therapeutics for RP and LCA.

Keywords: severe inherited blinding diseases; rhodopsin; molecular modelling; small-molecule agents; synthetic organic chemistry.

1. Introduction

The process of vision requires the transduction of environmental light into an electrical signal, that needs conversion by the retina into a suitable form that can be processed by the brain [1]. The step of light detection of this process is allowed by a series of G-protein-coupled receptors (GPCRs), called visual pigments, which are opsin proteins situated in the photoreceptive neurons of the retina [1]. In the healthy retina, absorption of visible light triggers a *cis-trans* isomerization of the chromophore 11-*cis*-retinal, covalently bound through a Schiff base link to opsin forming rhodopsin [2], starting the phototransduction cascade. After photoisomerization, all-*trans*-retinal is released from opsin and the 11-*cis* isomer is regenerated through a cycle of enzymatic reactions known as the visual cycle [3]. This physiological process requires folding of rhodopsin and its localisation from the endoplasmic reticulum (ER) to the outer segment membranes of photoreceptors, where, upon absorption of light, it activates the G-protein transducin [4]. The inability of rhodopsin to fold properly and to be trafficked to the outer segment membranes of photoreceptors is at the root of severe blinding conditions that can be classified as ocular protein conformational diseases [5]. One such disease is retinitis pigmentosa, RP, a common congenital eye dystrophy that affects 1 in 4,000 people. 40% of RP cases are caused by structurally destabilising mutations in the rhodopsin gene (RHO), such as P23H, which impair the correct folding and trafficking of rhodopsin to the membrane [6]. In addition, opsin folding and trafficking can also be impaired by the body's inability to synthesise 11-*cis*-retinal, which functions as a chemical chaperone for opsin and enables its proper folding and localisation to the outer segment photoreceptor membrane. This 11-*cis* retinal deficiency is the cause for ~ 30% cases of Leber's congenital amaurosis (LCA) [7]. LCA is the most severe retinal disfunction in infants, causing blindness before one year of age, and being responsible for 20% of children in schools for the blind. [8]. Both RP and LCA are severe, hereditary diseases that cause irreversible progressive vision impairment and eventually blindness. A significant proportion of both conditions is caused by the aggregation of unfolded opsin molecules, which accumulate in the ER,

inducing ER stress and culminating in the death of photoreceptor cells resulting in a progressive loss of vision [9]. Although gene therapy may be a possible treatment option in the future [10], a viable cure is still not available for these protein conformational diseases. Potential pharmacological treatments for these conditions, such as 9- or 11-*cis*-retinal precursors, are under investigation, but none of the strategies explored so far can interfere with the progression of retinal degeneration and the loss of photoreceptive neurons [6]. A possible approach to prevent opsin misfolding and promote its physiological trafficking to the outer photoreceptor cell membrane may be chemical chaperones. These are small molecules that can bind opsin, mainly at the level of the orthosteric binding site of 11-*cis*-retinal, and are then able to induce its proper folding and trafficking [11]. On top of retinoid analogues, such as 9-*cis*-retinoid derivatives which can preserve retinal health in mouse models [6], different chemical chaperones have recently been explored for their ability to bind wild-type and mutated opsins and induce their physiological trafficking, thus interfering with ER stress and death of photoreceptors. **Figure 1** summarises the chemical structures of the chromophore 11-*cis*-retinal (11-*cis*-RAL), of its locked analogue 11-*cis*-6-membered ring-retinal (11-*cis*-6mr-RAL), which shows therapeutic effects in some degenerative retinal diseases [12], and of non-retinoid compounds with therapeutic potential, reported to act as chemical chaperones for opsin [11, 13, 14].
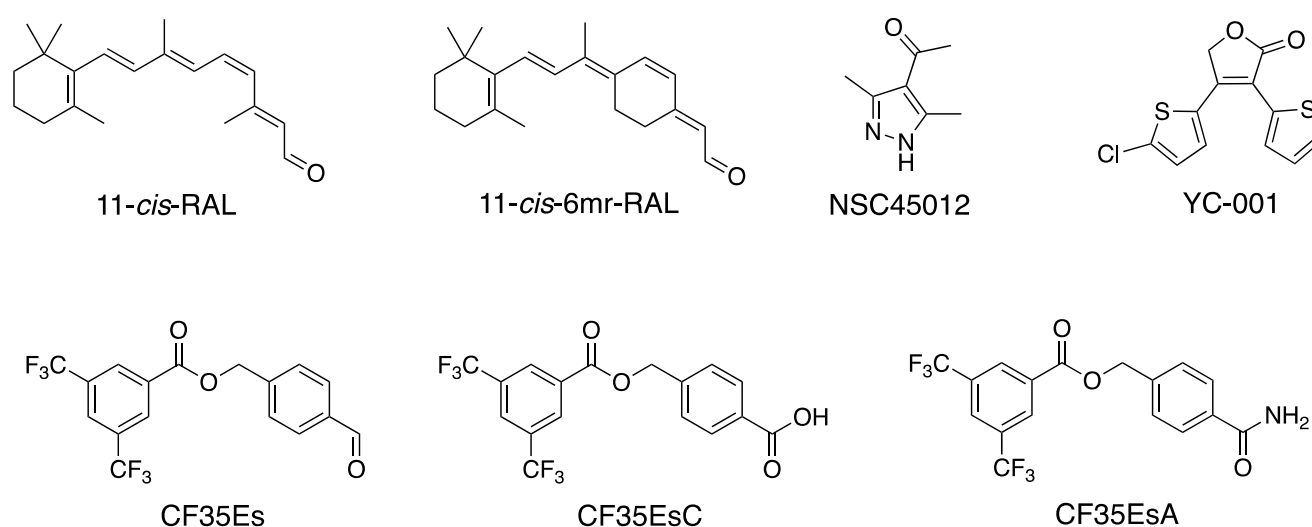
Figure 1. Chemical structure of opsin chromophore 11-*cis*-retinal (11-*cis*-RAL), its locked analogue 11-*cis*-6mr-RAL [12], along with previously reported pharmacological chaperones for opsin NSC45012 [11], YC-001 [13] and retinobenzaldehyde analogues CF35Es, CF35EsC, CF35EsA [14].

The aim of this work was to design and synthesise novel small molecules with the potential to act as chemical chaperones for opsin, as a means to induce its proper folding and trafficking in pathological conditions linked to destabilising opsin mutations (RP), or to a reduced presence of the endogenous chromophore 11-*cis*-retinal. These compounds could provide the basis to develop viable treatment options to prevent the death of photoreceptors and interfere with the loss of vision in patients affected by these inherited blinding diseases. To achieve this result, the structures of 11-cis-retinal, its locked analogue 11-cis-6mr-retinal, and previously reported retinobenzaldehydes were rationally modified, leading to the design of 49 new small-molecule compounds, all with an optimal predicted potential to bind the orthosteric site of rhodopsin according to molecular docking studies. One- to seven-step synthetic routes were optimised for the synthesis of the new target molecules, which were then evaluated for their ability to bind the main chromophore site of opsin in a competitive binding biochemical assay, and to induce the trafficking of P23H opsin from the ER to the outer cell membrane in a cell-based assay. Different new compounds were found to affect the rate constant k for the formation of 9-*cis*-retinal-rhodopsin, and/or to increase the trafficking of P23H opsin mutant, providing suitable starting points for the development of novel therapies for RP and LCA.

2. Results and discussion

2.1. Ligand-based rational design of novel potential opsin-binding compounds and molecular docking studies

In order to design novel potential ligands for opsin, the crystal structure of bovine rhodopsin, where opsin is covalently bound to 11-*cis*-retinal (PDB ID 1U19, 93% sequence identity with human rhodopsin) was first inspected for binding

interactions between opsin and the chromophore, and its overall occupation of the retinylidene orthosteric pocket, which are depicted in **Figure 2**.
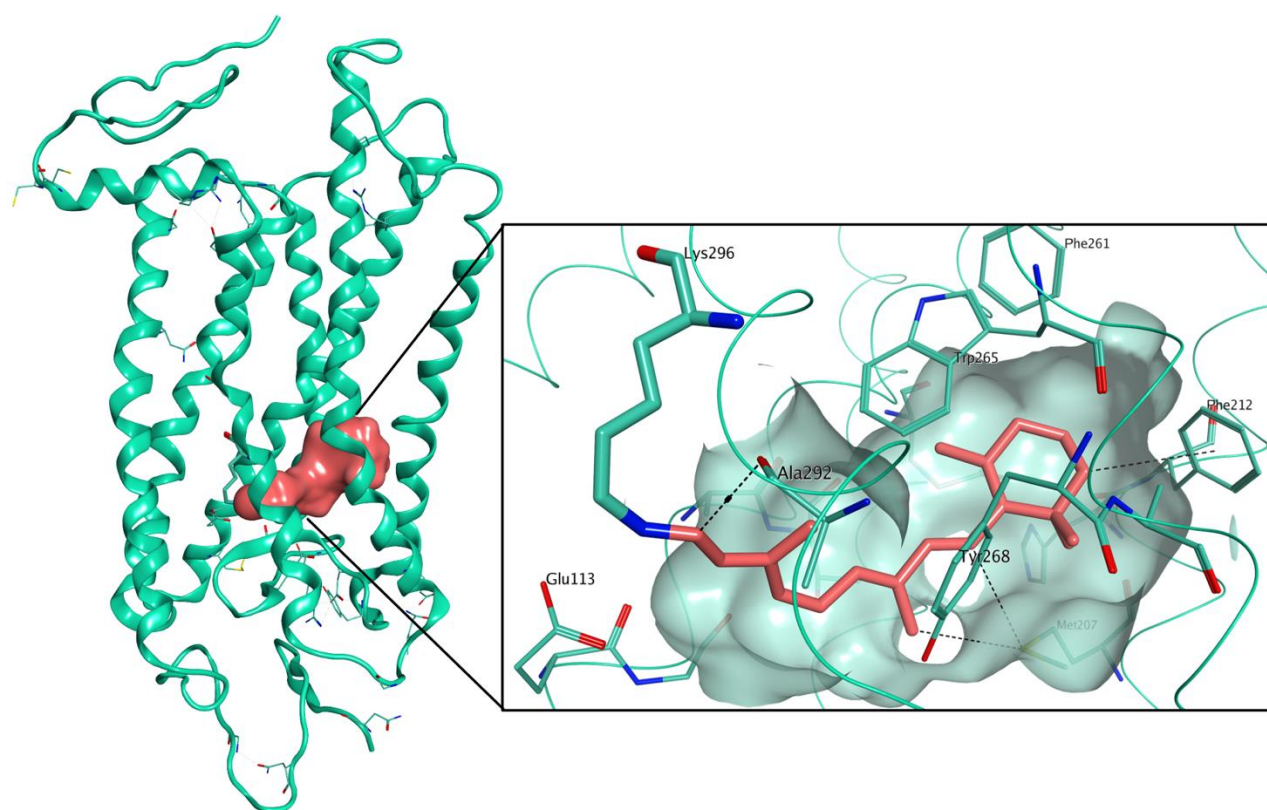

Figure 2. Crystal structure of bovine rhodopsin, where opsin is covalently bound to the chromophore 11-*cis*-retinal (carbon atoms in salmon). The binding site area is represented as molecular surface. Rhodopsin is represented with a green ribbon and carbon atoms in green.

The chromophore 11-*cis*-retinal is covalently bound to the orthosteric site by forming a Schiff base with Lys296. Additional interactions stabilize this binding and include a hydrogen bond between the imine carbon and the carbonyl of Ala292, and additional contacts between the ionone portion of the ligand and the hydrophobic residues of the binding site, including Met207, Phe212, Phe261, and Trp265. This hydrophobic area of the binding cleft acts as an essential recognition site for the ionone ring and for binding to this site, as confirmed by the ability of the shortened retinal derivative β-ionone (**Figure 3**), to competitively inhibit binding of 11-*cis*-retinal. β-Ionone binding however, which we previously investigated by molecular docking studies [15], does not induce any physiological effect on opsin trafficking [16-18].

Along with the binding of the endogenous ligand, the common structural features of 11-*cis*-retinal and different compounds known to competitively inhibit its binding to opsin were considered for the design of novel potential ligands for the orthosteric pocket, as depicted in **Figure 3**.
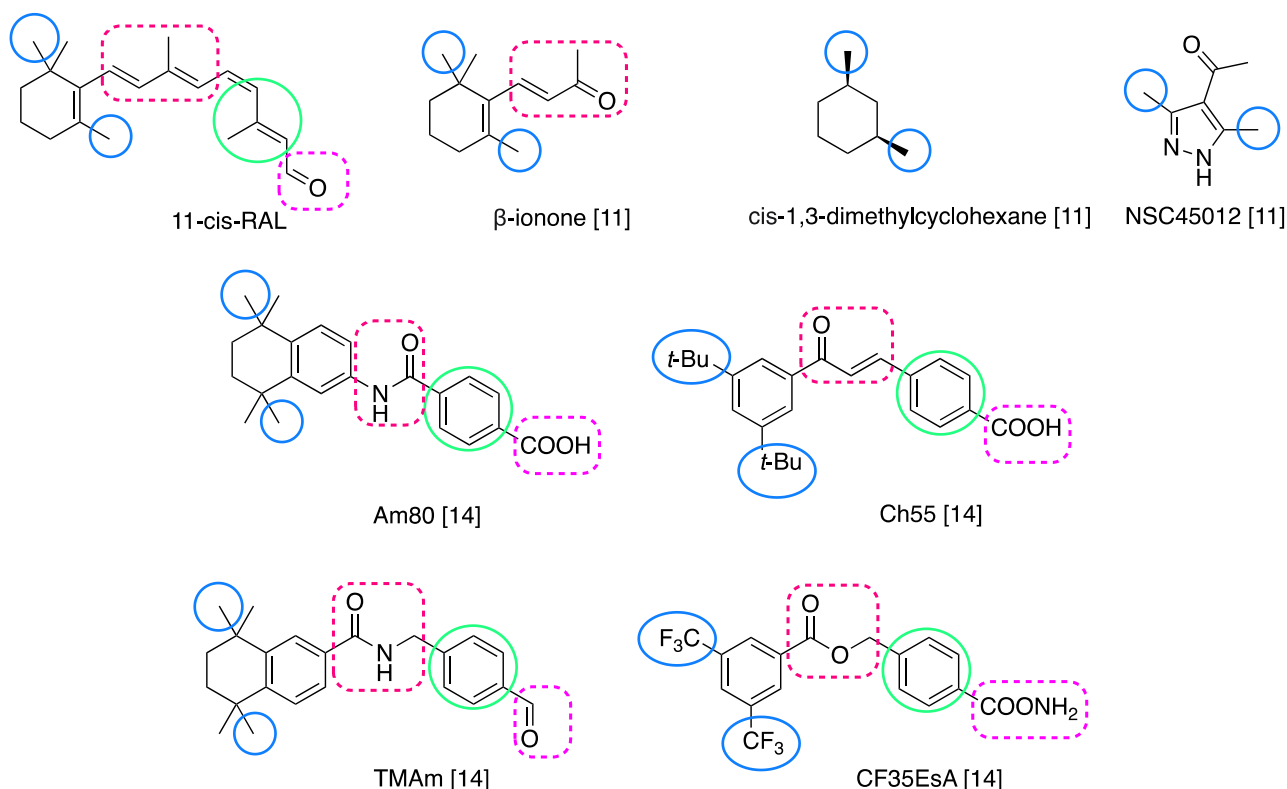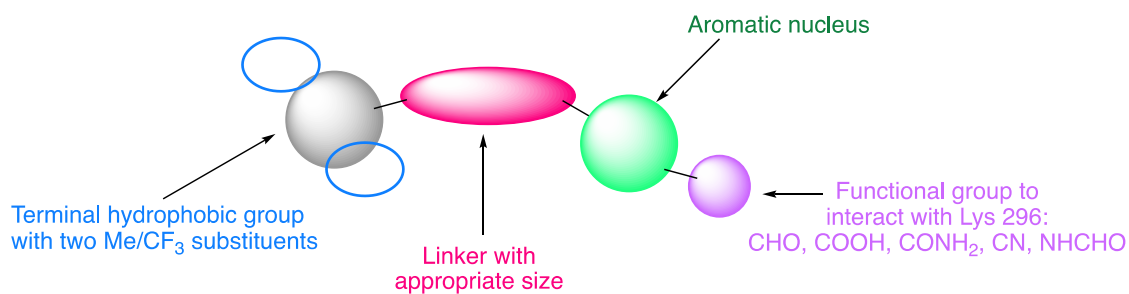
Figure 3. Chemical structures of small-molecule compounds reported to bind opsin and/or induce its proper folding and/or trafficking to the outer cell membrane. Structural features considered for the design of novel potential opsin ligands are highlighted by colored circles: a terminal hydrophobic group bearing two methyl or trifluoromethyl substituents on the left hand side of the scaffold (light blue), a central spacer of appropriate size (dotted magenta), a terminal aromatic nucleus on the right hand side of the structure (green), linked to a functional group that can react (CHO, CN, NHCHO) or interact (COOH, CONH₂) with Lys296 (dotted lilac).

Considering the features rationalized in Figure 3, eight new structural scaffolds were designed as potential chemical chaperones for opsin, as detailed in **Figure 4**.
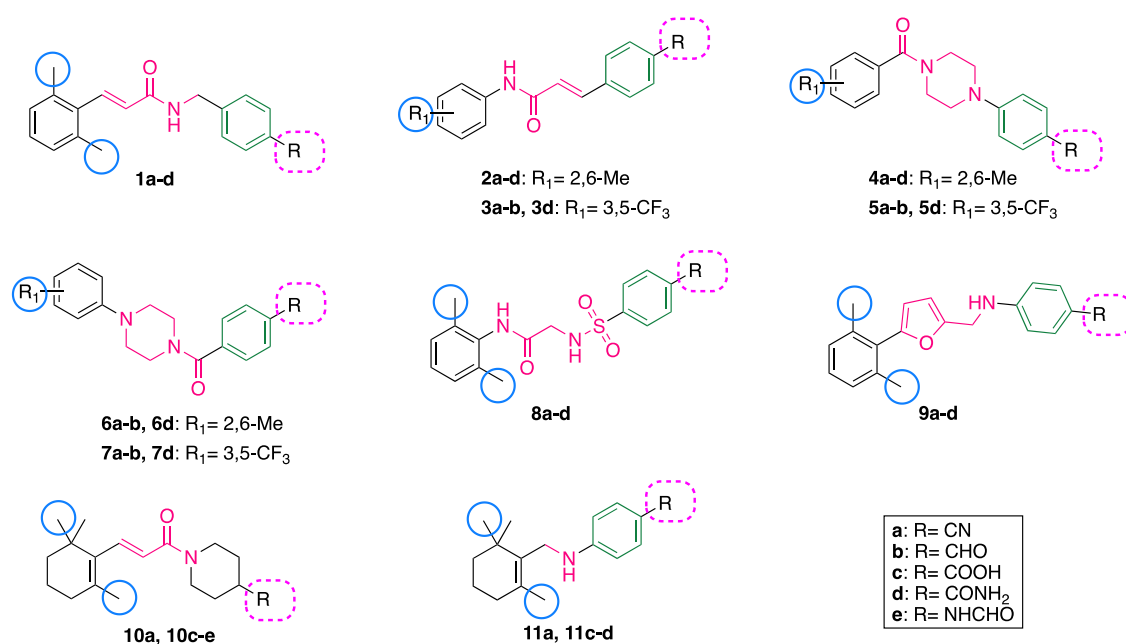
Figure 4. Chemical structures of the novel scaffolds designed as potential pharmacological chaperones for opsin, according to the features rationalized in **Figure 3**.

Most of chemical opsin chaperones reported to date share a common ability to bind the main chromophore site of the protein (orthosteric pocket), with a direct correlation between their ability to inhibit the binding of retinals to this pocket and their capacity to rescue misfolded opsins and induce their proper folding and trafficking to the outer cell membrane [11, 13]. As tool to predict the potential of our novel target compounds to bind opsin orthosteric pocket, and therefore their likelihood to act as chemical chaperones for this protein, molecular docking studies were performed for the novel target compounds **1-11** on the chromophore site of the 1U19 crystal structure, using the Glide SP software [19] (**Figure 5**). All the novel scaffolds are predicted to have an optimal occupation of rhodopsin orthosteric pocket, thus confirming their potential to act as chemical chaperones and enable the proper folding of the protein.
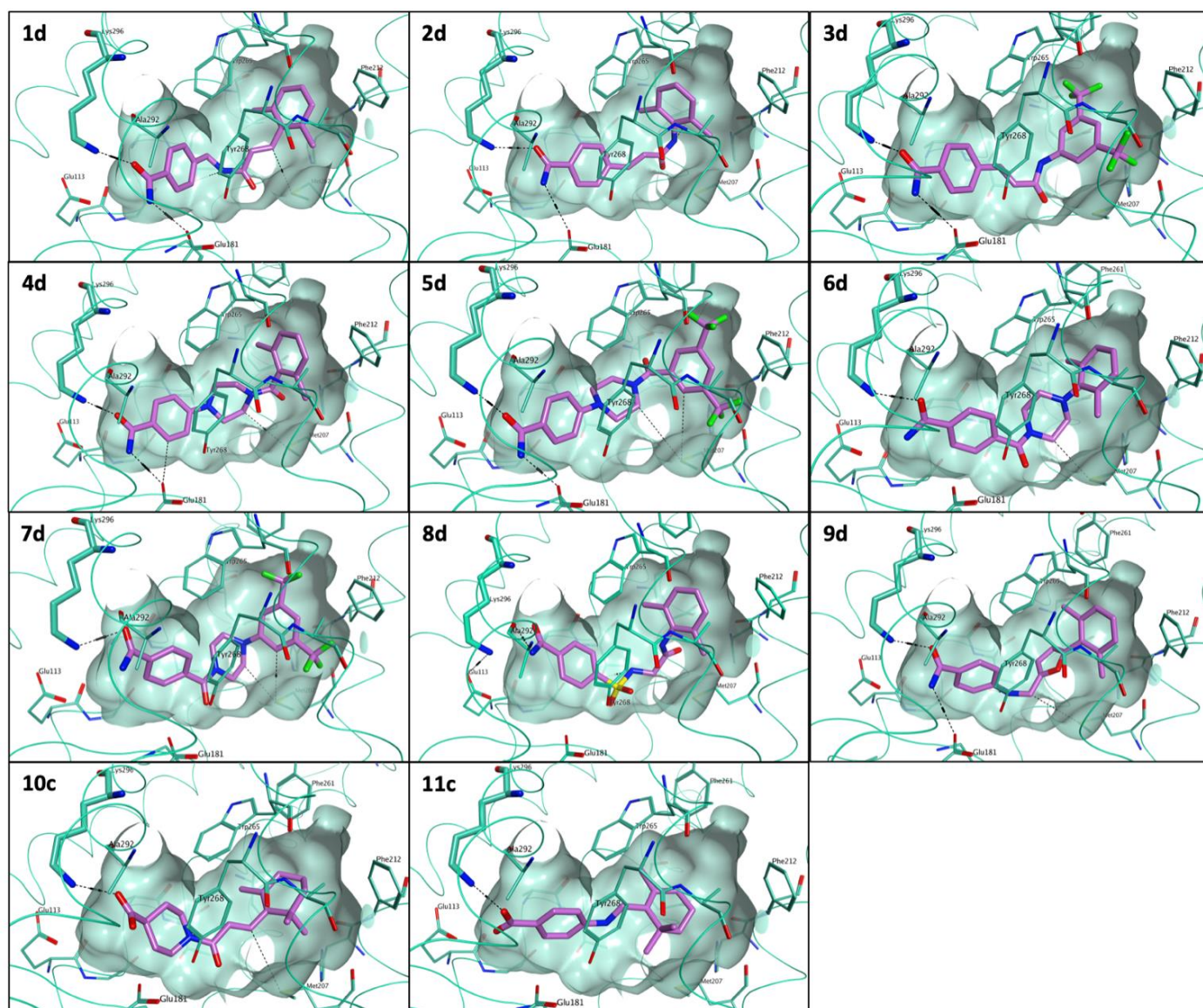
Figure 5. Predicted binding of selected analogues of the newly designed scaffolds **1-11** to the orthosteric pocket of rhodopsin crystal structure 1U19, analyzed with the molecular docking software Glide SP [19]. All the novel compounds are associated with an optimal predicted occupation of the main chromophore binding site, with an ideal overall fitting of the pocket, and the potential of forming direct contacts with Lys296, Glu181, and important hydrophobic residues exposed at the surface of the site, such as Ala292 and Met207. This optimal fit of rhodopsin orthosteric site confirms the potential of the novel scaffolds to act as chemical chaperones for the protein.

A further set of novel analogues was designed to replace the terminal group to interact with Lys296 with additional chemical functionalities, in addition to nitriles and aldehydes, with the potential to form a covalent bond with Lys296. Such molecules would generate a non-hydrolysable complex (irreversible ligands) upon binding non-covalently first, thanks to their good overall occupation of the orthosteric pocket of opsin. Once the reactive group is in the proper orientation, it would then be attacked by Lys296 to form a covalent bond with this residue selectively. To achieve this result, the insertion of a terminal acrylamide or trifluoromethyl-acrylamide group was planned in compounds **12-14** (**Figure 6**). Such groups are known for their ability to act as electrophilic Michael acceptors and covalently bind Cys, Lys or Tyr residues [20-23].

A.

B.
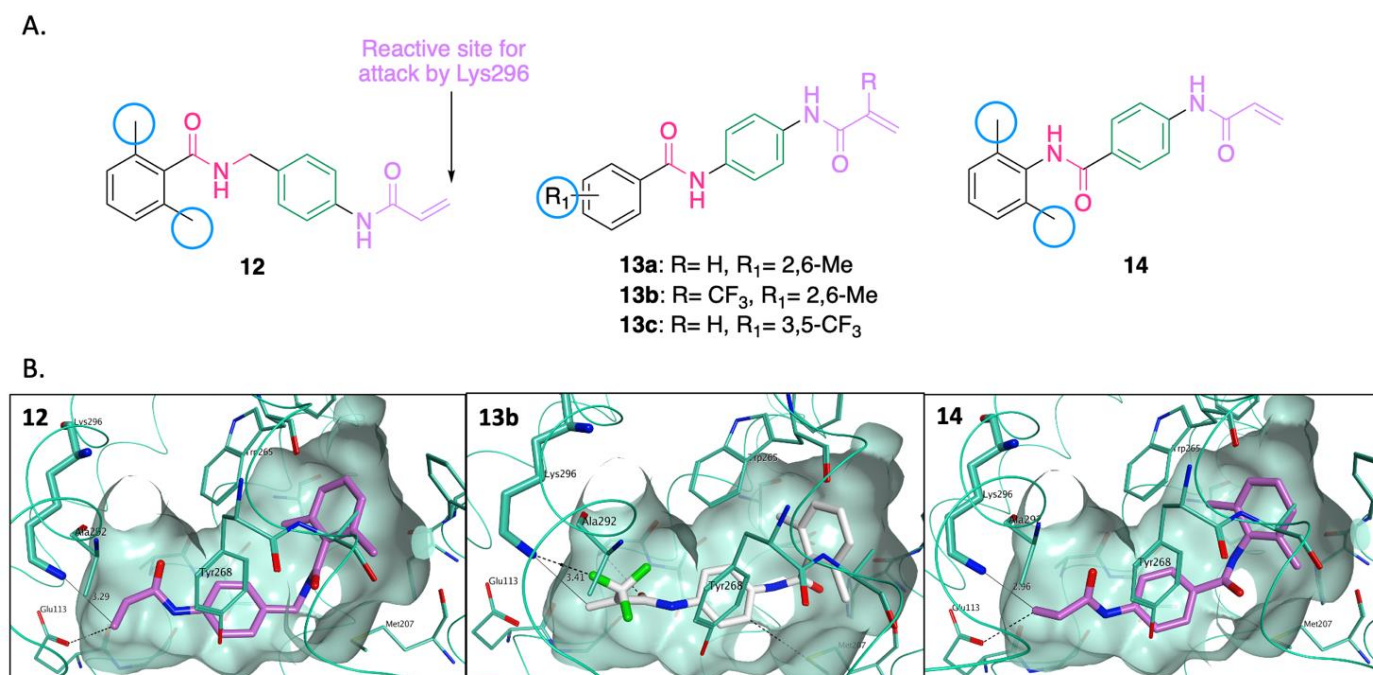
Figure 6. A. Chemical structures of newly designed acrylamide compounds **12-14**; and B. predicted binding to rhodopsin or-thosteric site (PDB ID 1U19) according to molecular docking studies performed with Glide SP [19] for **12**, **13b** and **14**. All the novel analogues designed are associated with an optimal fitting of the main chromophore binding pocket, with the reactive site of the acrylamide function in interacting distance from Lys296, potentially readily available for nucleophilic attack.

Finally, one last set of modified analogues were designed as derivatives of 11-*cis*-6mr-retinal, to maintain the terminal β-ionone portion and the function to target Lys296, mainly a aldehyde to form a covalent Schiff base bridge, while exploring different potential central cores between the two functionalities, such as a tetrahydroisoquinoline nucleus with a branched (**15**) or linear alkyl spacer (**16a-b**), or a piperidine nucleus with either an cyclic (**17**) or an unsaturated linear spacer (**18**). The newly designed analogues are shown in **Figure 7**, along with their predicted binding to the orthosteric pocket of rhodopsin crystal structure (PDB ID 1U19).

A.

B.
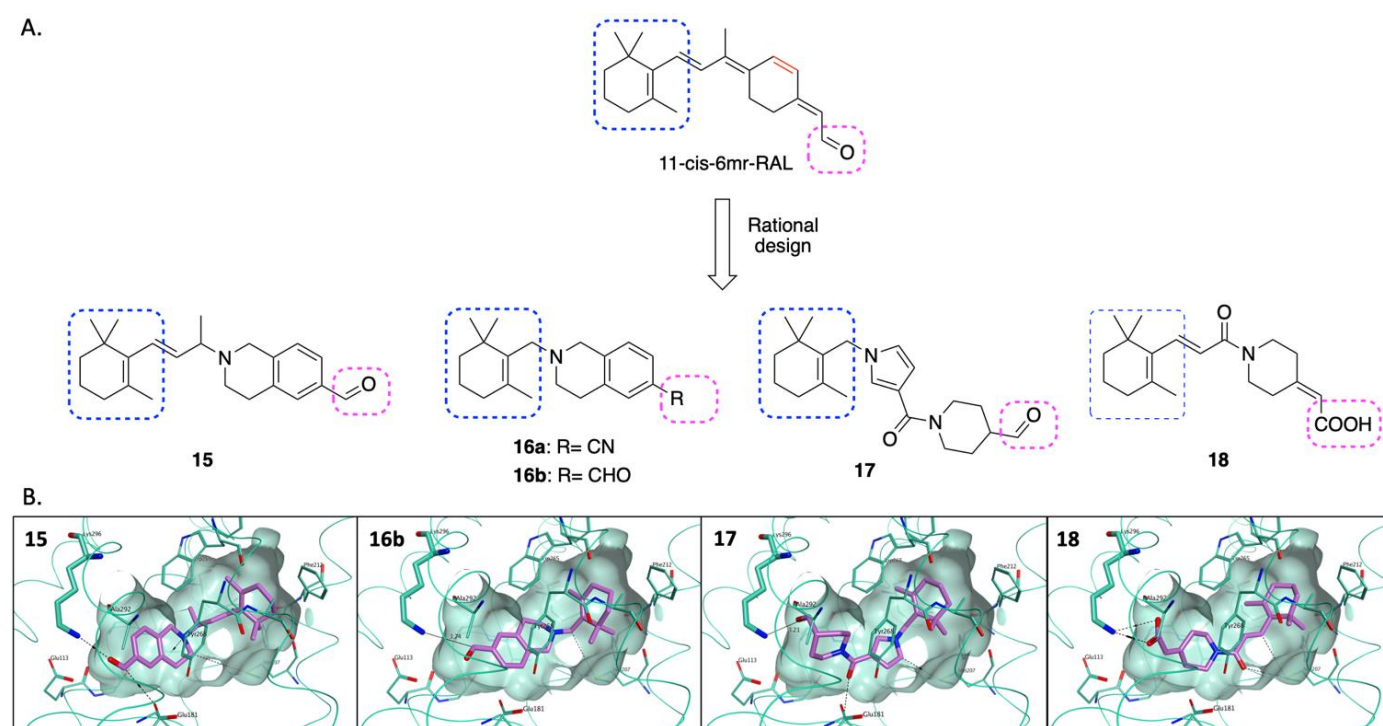
Figure 7. A. Chemical structures of newly designed compounds 15-18; and B. predicted binding to rhodopsin orthosteric site (PDB ID 1U19) according to molecular docking studies performed with Glide SP [19] for **15**, **16b**, **17** and **18**. All the novel analogues designed are associated with an optimal fitting of the main chromophore binding pocket, with the reactive site of the aldehyde/carboxylic acid group in close proximity to Lys296 (**15**, **16b**, **17**), potentially readily available for nucleophilic attack, or with the possibility to form direct hydrogen bonds or electrostatic interactions (**18**).

2.2. Synthesis of the new target compounds

All the newly designed small molecules were synthesized according to optimized organic chemistry strategies.

The synthesis of compounds **1a-7a** is summarized in **Scheme 1**. Briefly, **1a** was prepared according to a three-step route, starting with a Wittig reaction between aldehyde **19** and phosphorane **20** [24] to give unsaturated ester **22**, which was readily hydrolyzed to the corresponding acid **23** with LiOH in a 1:2 mixture THF/H2O. **23** was then coupled with substituted benzylamine **24** using the TBTU amide coupling agent [25], in the presence of DiPEA as a base. For the preparation of **2a** and **3a**, a Doebner-Knoevenagel condensation [26], between benzaldehyde **25** and malonic acid **26**, gave intermediate acid **27**, which was then treated with either aniline **28** or **29** in the presence of TBTU and DiPEA to give the amide group in the target final compounds. Another two-step synthetic route was applied for the preparation of target molecules **4a**, **5a**, **6a** and **7a**, using a Buchwald-Hartwig cross-coupling reaction in the first stage [27], between piperazine **31** and differently substituted aryl bromides **30**, **35** and **36**, to give amines **32**, **38** and **39**. These intermediates were then treated with the differently substituted benzoic acids **33**, **34** or **40** according to another TBTU-assisted amide coupling reaction, to provide the desired nitrile derivatives **4a-7a** in good yields after column chromatography purification.
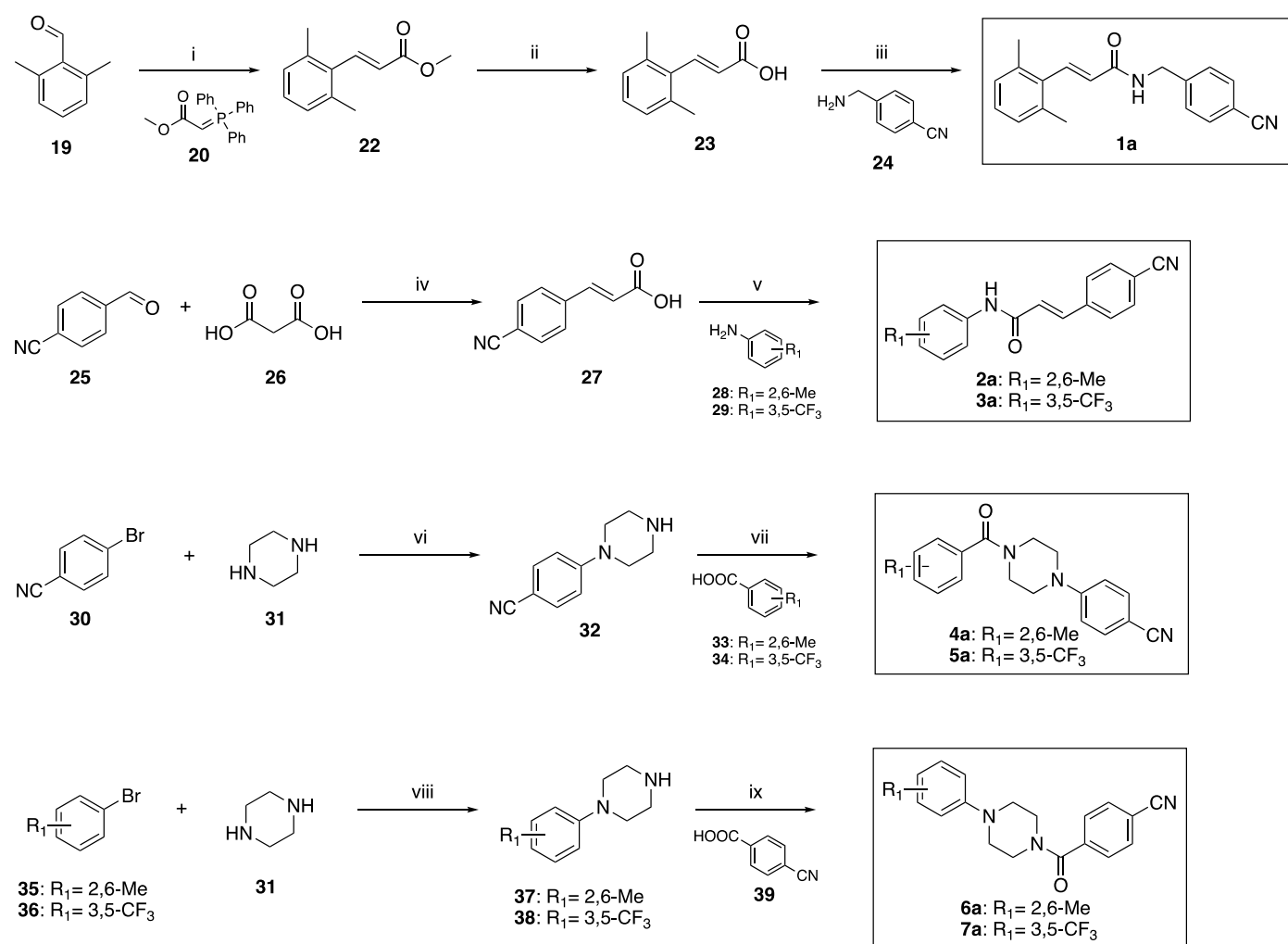
Scheme 1. Preparation of target compounds **1a-7a**. *Reagents and conditions*: (i) PhMe, reflux 4h, r.t. o.n. (85%); (ii) LiOH, THF, H2O, 85 °C, o.n. (83%); (iii) TBTU, DiPEA, DMF, 0 °C to r.t., 36 h (73%); (iv) cat. piperidine, Pyr, reflux, 4 h (87%); (v) TBTU, DiPEA, DMF, 0 °C to r.t., 36 h (67-75%); (vi) BINAP, Pd2(dba)3, *t*-BuONa, PhMe, 85 °C, o.n. (79%); (vii) TBTU, DiPEA, DMF, 0

°C to r.t., 36 h (71-77%); (viii) BINAP, Pd$_2$(dba)$_3$, *t*-BuONa, PhMe, 100 °C, 24 h (45-62%); (ix) TBTU, DiPEA, DMF, 0 °C to r.t., 36 h (84-92%).

Scheme 2 summarises the synthesis of target molecules **8-11**, **1b-7b**, **1c**, **2c**, **4c**, **8c**, and **1d-8d**.
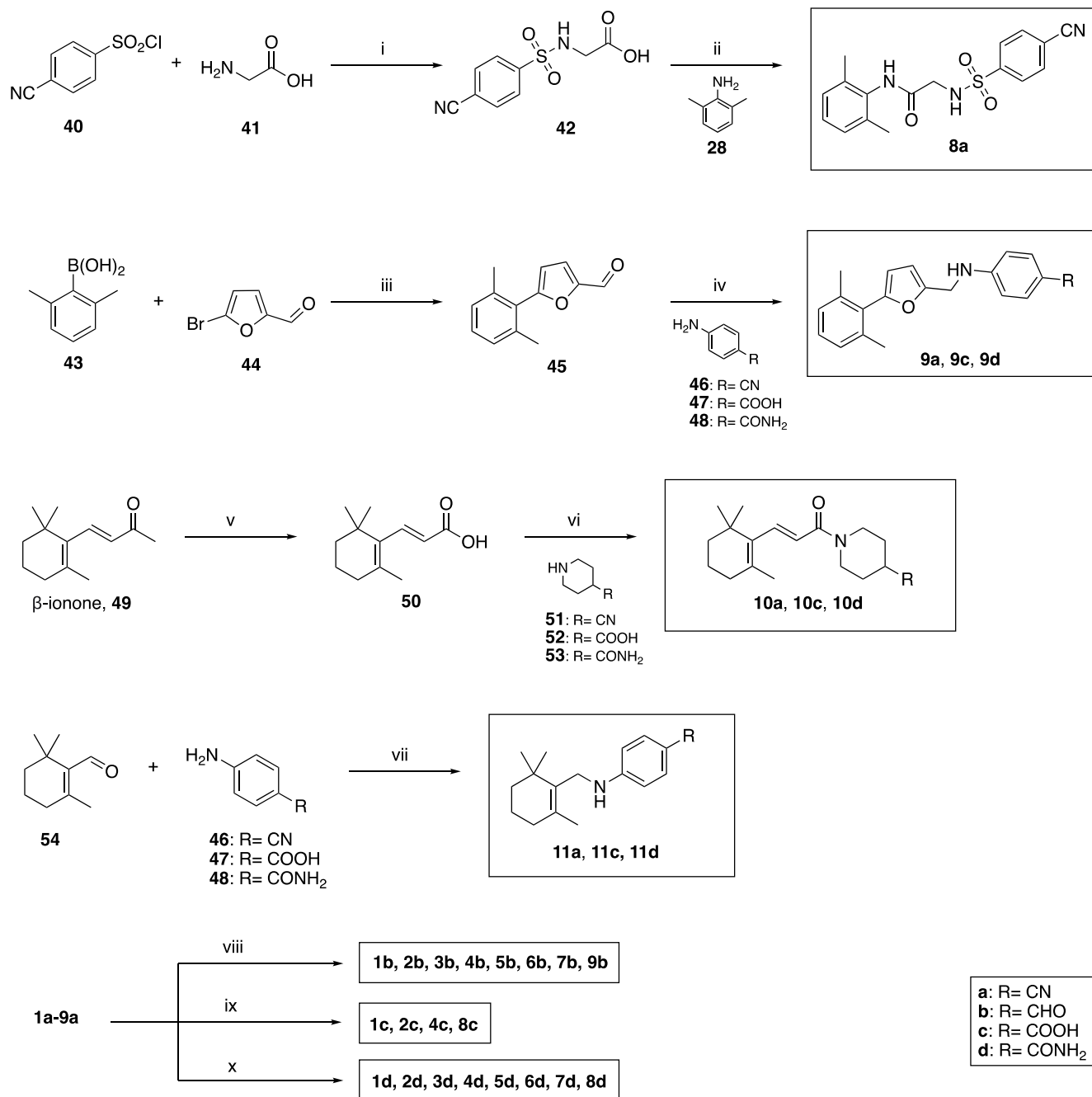
Scheme 2. Preparation of target compounds **8-11**, **1b-7b**, **1c**, **2c**, **4c**, **8c**, and **1d-8d**. *Reagents and conditions*: (i) NaOH, DiPEA, H$_2$O, Me$_2$CO, 0 °C to r.t., 1 h (90%); (ii) a. (COCl)$_2$, cat. DMF, DCM, 0 °C to r.t., 2 h; b. Et$_3$N, DCM, 0 °C to r.t., 2 h (73%); (iii) Pd(PPh$_3$)$_4$, Na$_2$CO$_3$, THF, H$_2$O, 60 °C, 24 h (65%); (iv) a. MeOH, reflux, 6 h; b. NaBH$_4$, AcOH, 0 °C to r.t., 1 h (64-89%); (v) NaOCl, MeOH, 0 °C to r.t., 24 h (98%); (vi) TBTU, DiPEA, DMF, 0 °C to r.t., o.n. (69-82%); (vii) a. MeOH, reflux, 24 h; b. NaBH$_4$, AcOH, 0 °C to r.t., 3 h (29-47%); (viii) cat. PtO$_2$, 80% aq. HCOOH, 60 °C, 24 h OR DIBAL-H, PhMe, -78 °C to r.t., 10 min. (48-69%); (ix) H$_2$SO$_4$, H$_2$O, reflux, o.n. OR NaOH, H$_2$O, EtOH, 90 °C, o.n. (51-98%); (x) 6N NaOH, 30% H$_2$O$_2$, THF, EtOH, r.t., 48 h OR *t*-BuOK, *t*-BuOH, r.t., o.n. (49-68%).

Preparation of sulfonamide analogue **8a** was achieved by reacting sulfonyl chloride **41** with β-alanine **42** in the presence of NaOH and DiPEA to give intermediate **43**, which was then combined with aniline **28** according to another TBTU-

promoted amide coupling reaction. The final target molecules **9a**, **9c** and **9d** were also prepared following a two-step synthetic route, which started with a Suzuki coupling reaction [28], between boronic acid **44** and aromatic bromide **45**, to afford the aldehyde intermediate **46**, which was then reacted with anilines **47-49** according to a reductive amination, using NaBH₄ as reducing agent. The final reductive amination to obtain **9a** was performed in MeOH in two stages, allowing for the formation of the imine first, and then reducing it by addition of NaBH₄, as attempts to perform a one-pot reaction using NaBH₃CN as reducing agent did not lead to the formation of the desired reduction product. Preparation of the target compounds **10a**, **10c** and **10d** was achieved starting with the oxidation of β-ionone into the unsaturated acid **50** using NaOCl as oxidizing agent, followed by treatment of this acid intermediate with differently substituted, racemic piperidines **51-53**, according to a TBTU-assisted coupling reaction, which afforded the final target molecules in good yields after chromatographic purification. The shorter target molecules **11a**, **11c** and **11d** were obtained according to a two-stage reductive amination reaction between β-cyclocitral **54** and differently substituted anilines **47-49**, by preparing the imine in refluxing MeOH first, and then adding the NaBH₄ reducing agent to the reaction mixture. Finally, nitrile compounds **1a-9a** were converted into the corresponding aldehyde, carboxylic acid or carboxamide target compounds. Aldehydes **1b-7b** and **9b** were obtained by reduction of the corresponding nitriles **1a-7a** and **9a**, either in aqueous formic acid in the presence of catalytic amounts of PtO₂, or using DIBAL-H in toluene. Carboxylic acids **1c**, **2c**, **4c** and **8c** were prepared following a reduction of the corresponding cyano compounds **1a**, **2a**, **4a** and **8a**, using sulfuric acid in boiling water, or NaOH in an EtOH/water mixture, while carboxamides **1d-8d** were isolated after reducing the corresponding nitriles **1a-8a** either with a mixture of NaOH and H₂O₂ in THF/EtOH, or using *t*-BuOK in *t*-BuOH.

Attempts to prepare the target aldehyde analogue **8b** from the corresponding nitrile **8a**, either in aqueous formic acid using catalytic amounts of PtO₂ or using DIBAL-H in either toluene or dichloromethane, provided only traces of the desired product. Therefore, the synthetic approach to obtain this analogue was modified to use a starting material that already features the desired aldehyde group (sulfonyl chloride **58**), as described in **Scheme 3**, which also shows the preparation of **10e**.
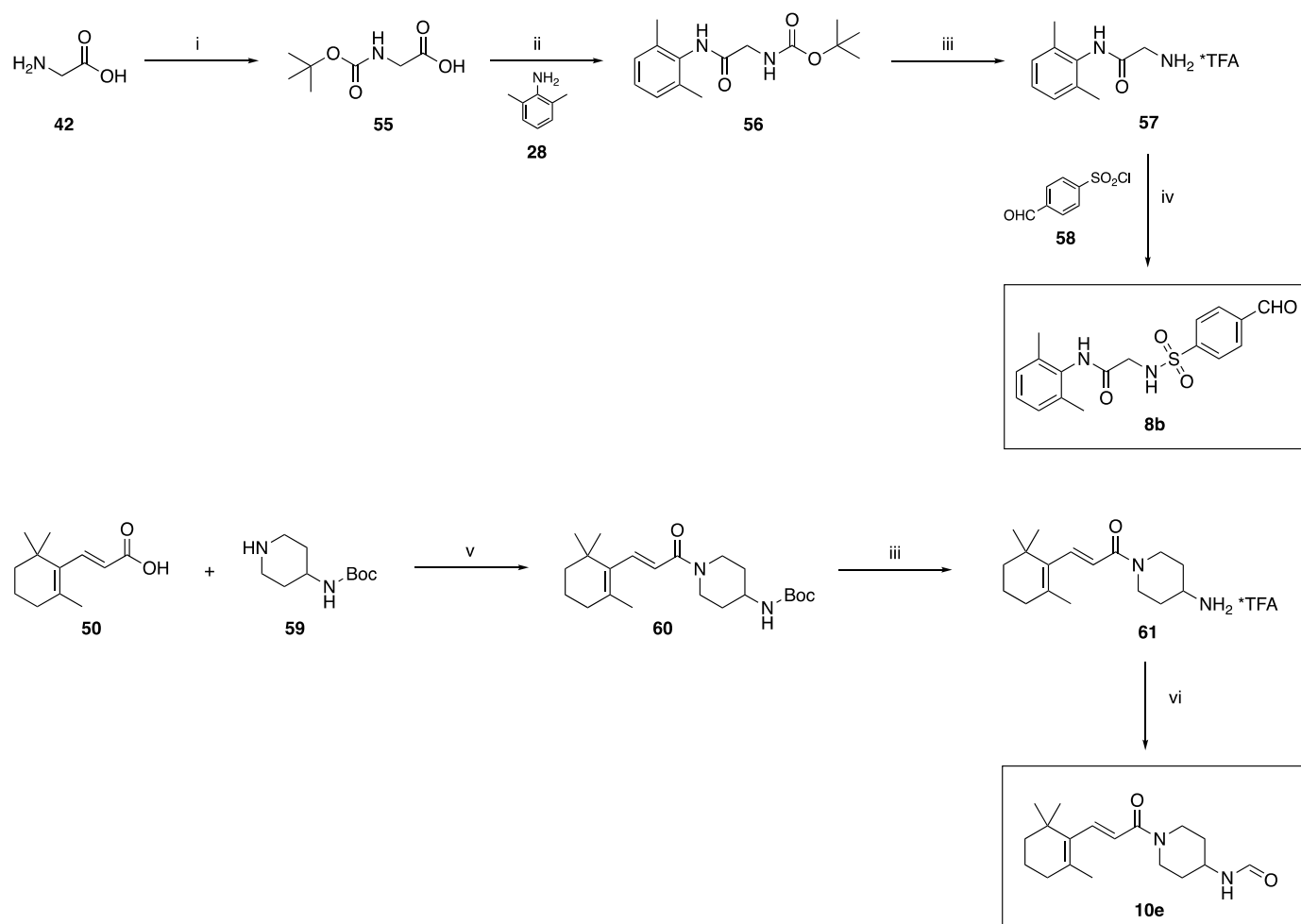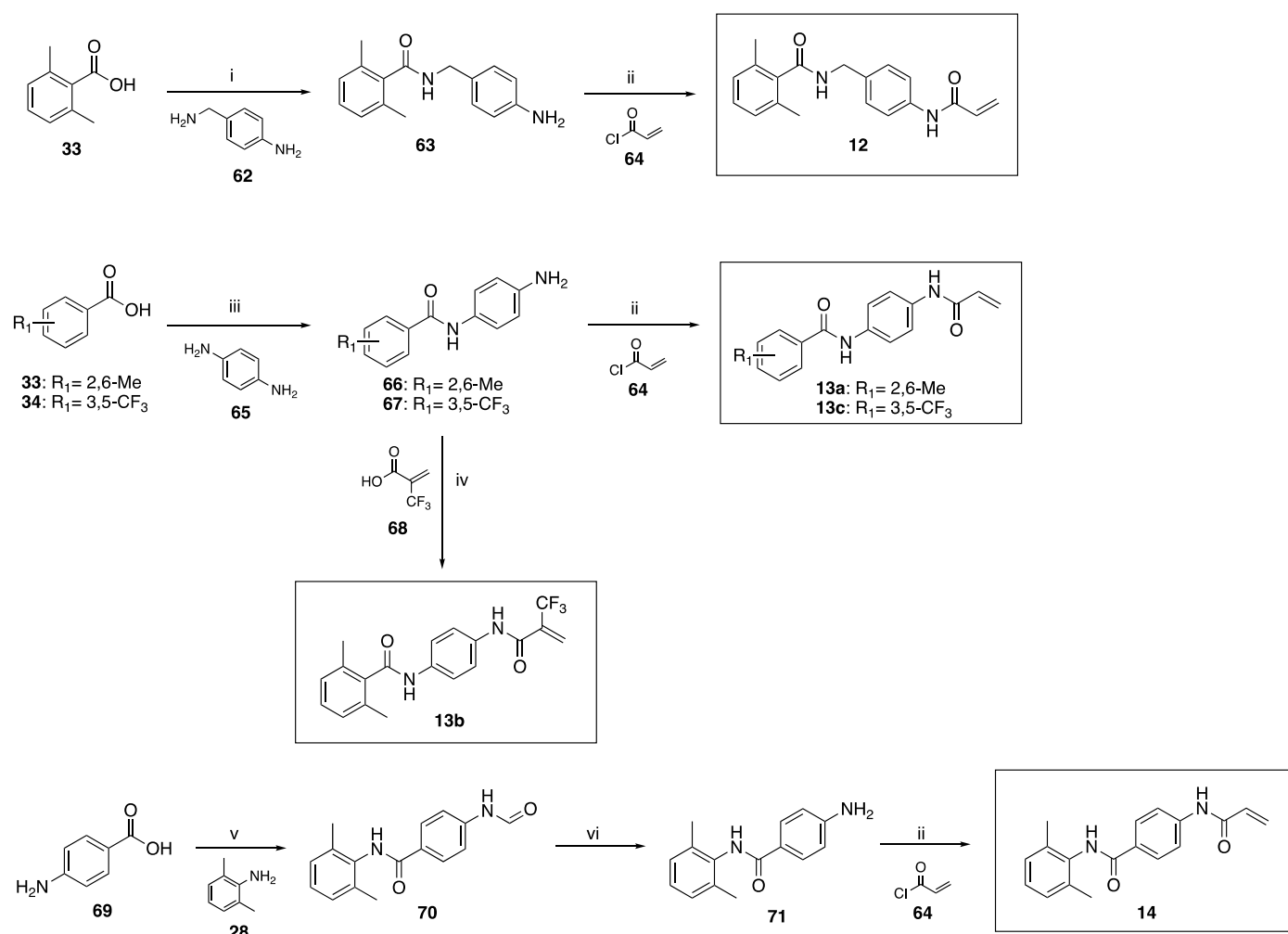

Scheme 3. Preparation of target compound **8b** and **10e**. *Reagents and conditions*: (i) Boc₂O, NaOH, H₂O, Me₂CO, H₂O, 0 °C to r.t.,

2 h (99%); (ii) TBTU, DiPEA, DMF, 60 °C, 24 h (82%); (iii) TFA, DCM (1:1, v/v), 0 °C to r.t., 2 h (quant.); (iv) Et₃N, DCM, 0 °C to r.t., 30 min (67%); (v) TBTU, DiPEA, DMF, 0 °C to r.t., 6 h (99%); (vi) ethyl formate, reflux, 16 h (66%).

The route to obtain **8b** began with the protection of the amine group of β-alanine **42** with the Boc protecting group [29], which enabled to react the carboxylic acid in **55** with aniline **28** according to a TBTU-assisted coupling reaction, to give the amide intermediate **56**. Removal of the Boc protecting group using TFA gave the TFA salt of the free amine **57**, which was finally reacted with sulfonyl chloride **54** in the presence of Et₃N, to give the desired final product **8b** in good yield.

Preparation of **10e** was achieved starting with an amide coupling reaction between the unsaturated carboxylic acid **50** and commercially available, Boc-protected 4-aminopiperidine **59**, which afforded the protected intermediate **60** in almost quantitative yield. Removal of the Boc protecting group in a 1:1 mixture TFA/DCM afforded the TFA salt of the free amine group in **61**, which underwent a final N-formylation in refluxing ethyl formate to give the target product **10e** in good yield.

The synthetic preparation of target acrylamide compounds **12-14** is summarized in **Scheme 4**.

Scheme 4. Preparation of target compounds **12-14** *Reagents and conditions*: (i) TBTU, DiPEA, DMF, 0 °C, 3 h (61%); (ii) DiPEA, THF, 0 °C to r.t., 1 h (57-68%); (iii) TBTU, DiPEA, DMF, 0 °C to r.t., o.n. (76-95%); (iv) TBTU, DiPEA, DMF, 0 °C to r.t., 3 h (35%); (v) a. (COCl)₂, DMF, DCM, 0 °C to r.t., 2 h; b. Pyr, DCM, 0 °C to r.t., 2 h; (vi) 1,2-ethylendiamine, EtOH, reflux, 6 h (71% over two steps).

12-13 were prepared according to a two-step approach, starting with a TBTU-assisted amide coupling reaction between the differently substituted benzoic acids **33-34** and either *para*-aminobenzylamine **62** or *para*-phenylendiamine **65**, to obtain intermediate anilines **63**, **66** and **67**, which were then treated with acryloyl chloride **64** in the presence of DiPEA to give the target final molecules **12**, **13a** and **13c**. **13b** was instead obtained by reacting intermediate **66** with 2-(trifluoromethyl)acrylic acid **68** in the previously adopted TBTU-assisted conditions for amide coupling reactions. A three-step approach was applied instead for **14**. *para*-Aminobenzoic acid **69** was converted into the corresponding acyl chloride

using oxalyl chloride in the presence of DMF, which acted as a solvent and formylating agent for the free amine group. Intermediate formylated amide **70** was obtained after treating *in situ* the resulting acyl chloride with aniline **28**, in the presence of pyridine as a base. The formyl protecting group was removed by refluxing **70** in EtOH in the presence of 1,2-ethylendiamine to give the final intermediate **71**, which was then reacted with acryloyl chloride **64** to give the desired product **14** in good yield.

Scheme 5 summarizes the synthesis of target compound **15** and the first attempts to obtain **16b**.
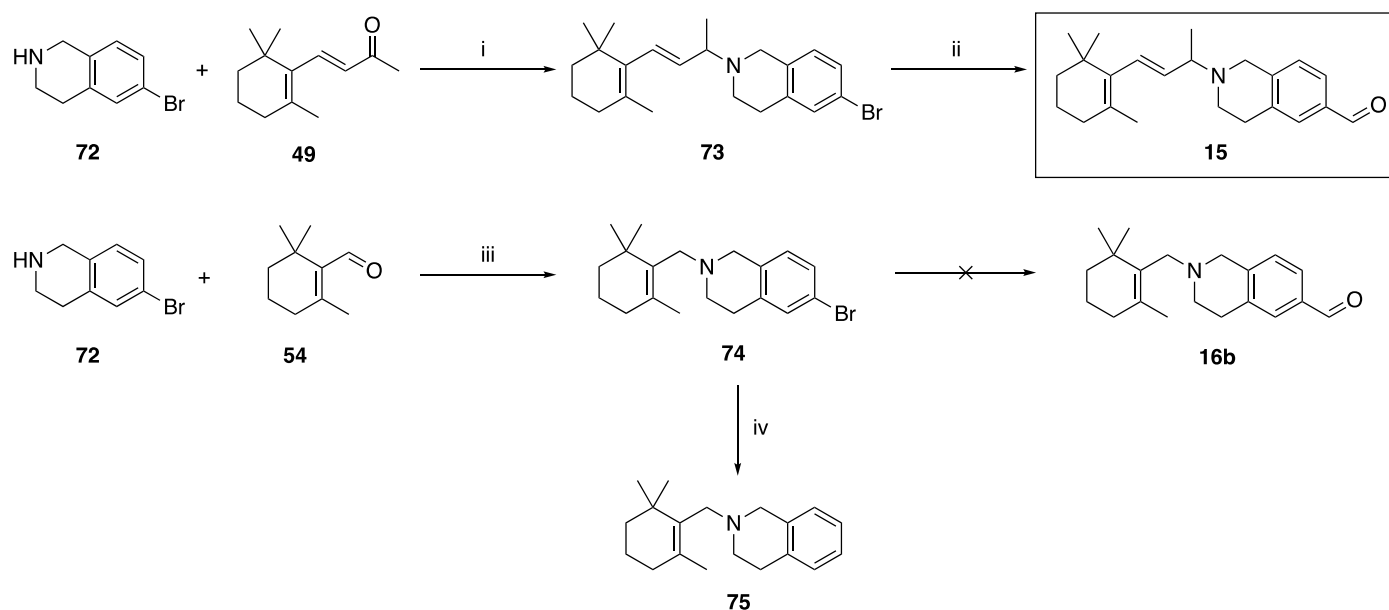

Scheme 5. Preparation of target compound **15** and early attempts for **16b**. *Reagents and conditions*: (i) a. Ti(OiPr)₄, 75°C, 3h; b. NaBH₃CN, EtOH, r.t., 24 h (89%); c) *t*-BuLi, DMF, Et₂O, -78 °C, 30 min (22%); (iii) NaBH(OAc)₃, EDC, r.t., 16 h (54%); (iv) *t*-BuLi, DMF, THF, -78 °C, 30 min (8%).

For the synthesis of **15**, a reductive amination reaction was performed between β-ionone and 6-bromo-tetrahydroiso-quinoline (6-Br-THIQ) **72**. Initially, sodium triacetoxyborohydride was used as reducing agent in the presence of AcOH in 1,2-dichloroethane (EDC) [30-31]. However, after 24 h at room temperature only the two starting materials were observed. The reaction was heated to reflux, but after 16h the N-acetylated form of THIQ was detected. A modified procedure was then attempted, using NaBH₄ as reducing agent in the presence of AcOH in MeOH. In these conditions, the reduced hydroxy derivative of β-ionone was the only product observed [32]. As an alternative strategy, a methodology for the synthesis of N-alkyl THIQ derivatives via formation of an iminium-titanium (IV) complex intermediate was attempted [33], performing this reductive amination in the presence of NaBH₄ and Ti(Oi-Pr)₄. Unfortunately, only the starting material β-ionone was recovered in these conditions. However, by replacing the NaBH₄ reducing agent with the more selective NaBH₃CN, the desired intermediate **73** was finally obtained in 89% yield. By reacting **73** with DMF in presence of *t*-BuLi [34], the bromine was replaced with the target aldehyde moiety so that the final product **15** could be successfully isolated.

For the preparation of the target final compound **16b**, a reductive amination performed in the presence triacetoxyboro-hydride in EDC was identified as an efficient methodology to obtain intermediate **74** from 6-Br-THIQ **72** and β-cy-clocitral **54**, thanks to the more reactive aldehyde function compared to the ketone in β-ionone. However, several attempts to synthesize **16b** in the presence of an organolithium compound and an aldehyde source were unsuccessful. Initially, the same conditions adopted for the preparation of **15** were applied [34], but the only product observed was the unsubstituted analogue **75**. The same reaction was then attempted by increasing the equivalents of DMF, by pro-longing the reaction time, and by replacing DMF with *N*-formylpiperidine as the carbonyl source [35], but all these attempts yielded **75** as the only isolated product, obtained in low yield. An alternative pathway was therefore envisaged for **16b**: in order to avoid the replacement of the aromatic bromine with a carbonyl, the use of a nitrile moiety on the THIQ scaffold was planned, followed by conversion into an aldehyde group, according to the retrosynthetic approach described in **Figure 8**. According to this retrosynthesis, the desired final product **16b** would be obtained by coupling β-

cyclocitral with the protected form (**77**) of tetrahydroisoquinoline-6-carbaldehyde **78**, which could in turn be obtained from the reduction of the corresponding nitrile derivative **79**.
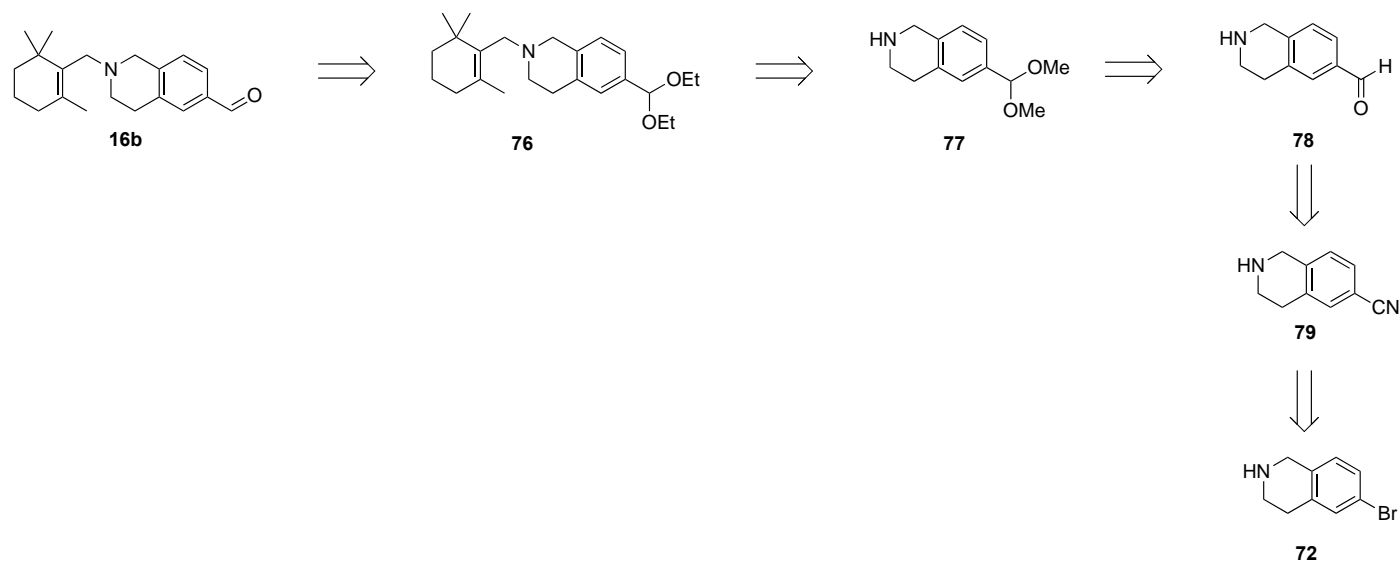
Figure 8. Modified retrosynthetic strategy for the synthesis of **16b**.

First, 6-CN-THIQ **79** needed to be prepared (**Scheme 6**), therefore 6-Br-THIQ **72** was reacted with Zinc cyanide under microwave irradiation in the presence of tetrakis(triphenylphosphine)palladium(0) as a catalyst in DMF [36]. Unfortunately, **79** was obtained with a very low 8% yield in these conditions, but performing the same reaction in a sealed tube at 150 °C afforded the desired product **76** in an improved 56% yield. However, this reaction proved to be reproducible only working on a small scale, and *N*-aldehyde-THIQ derivatives were also formed due to the use of DMF as a solvent. Nonetheless, the reduction of the nitrile group into an aldehyde was attempted on **76** using DIBAL-H as reducing agent [37], but isolation of the aldehyde derivative **75** could not be achieved. Protection of the NH group of 6-Br-THIQ **69** was therefore carried out to prevent the aforementioned issues (**Scheme 6**). After an almost quantitative Boc protection reaction to afford **80** [38], the formation of the nitrile derivative **81** was achieved with an improved 71% yield, and its reduction to the corresponding aldehyde derivative **72** was smoothly achieved with a 50% yield. However, the following aldehyde protection to obtain **80**, performed in the presence of trimethyl orthoformate [39], failed. Accordingly, we envisaged to start by performing first a reductive amination between β-cyclocitral **54** with 6-CN-THIQ **79**, followed by the reduction of the nitrile group to obtain the final product **16b** (**Scheme 6**). To achieve this result, compound **80** was deprotected in order to make the NH group available for alkylation in **79**. A reductive amination between **79** and **54** was subsequently performed in the presence of NaBH₃CN in EDC, affording the target compound **16a** in low yield, enabling the final nitrile reduction to be performed. **16a** was treated with DIBAL-H at -20 °C to finally afford the desired target compound **16b** in 20% yield.
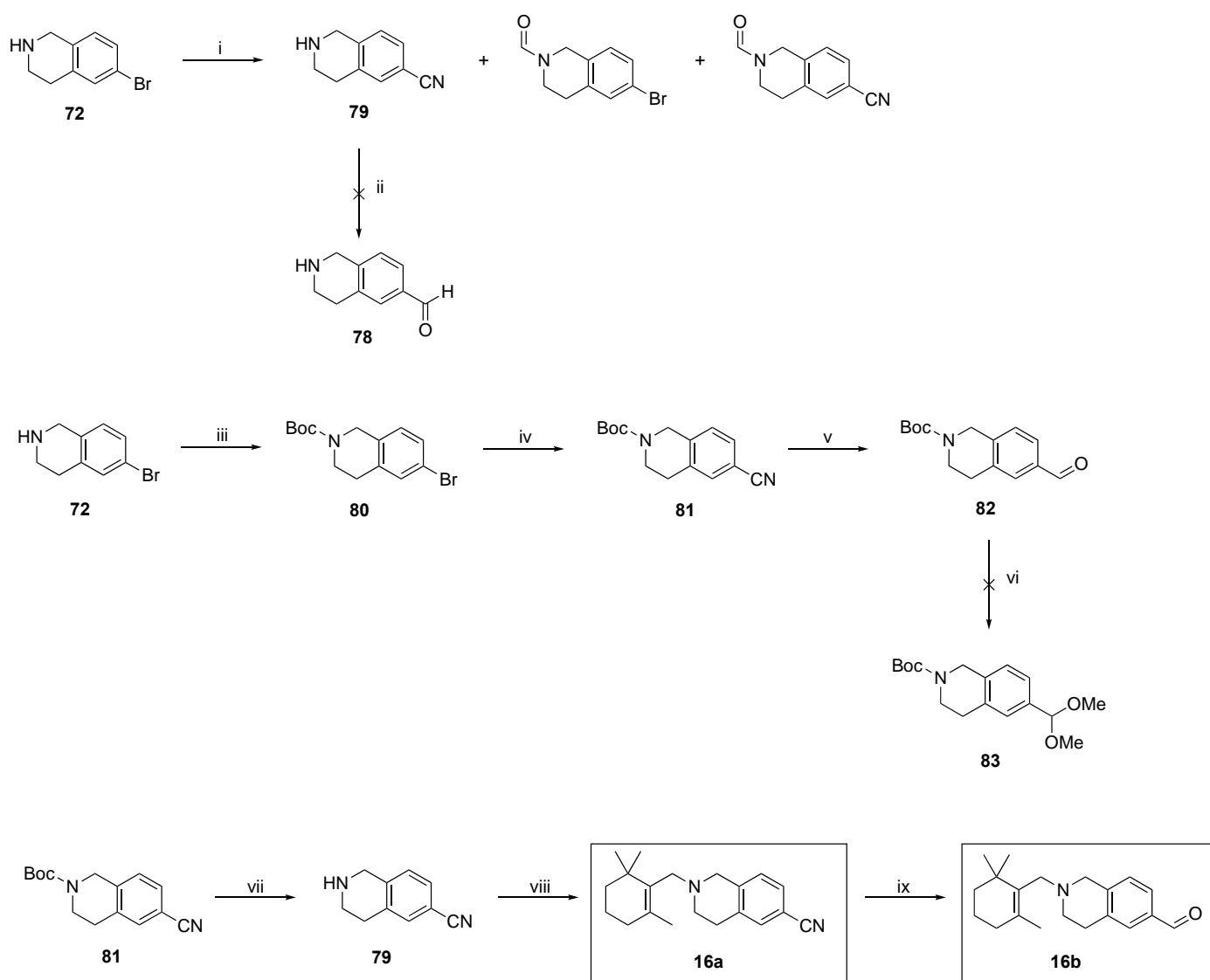
Scheme 6. Further attempts for the synthesis of **16b**. *Reagents and conditions*: (i) Zn(CN)₂, Pd(PPh₃)₄, DMF, 150 °C, sealed tube, 1.5 h (56%); (ii) DIBAL-H (1M in PhMe), PhME, -20°C to 0°C, 2 h (traces); (iii) Boc₂O, CH₂Cl₂, r.t., 2 h (98%); (iv) Zn(CN)₂, Pd(PPh₃)₄, DMF, 150 °C, sealed tube, 1.5 h (71%); (v) DIBAL-H (1M in PhMe), PhMe, -20 °C to 0 °C, 2 h (50%); (vi) CH(OCH₃)₃, *p*-TsOH, MeOH, reflux, 16 h (traces); (vii) TFA/CH₂Cl₂ (1:1, v/v), 0 °C, 2 h (quant.); (viii) β-cyclocitral **54**, NaBH₃CN, EDC, r.t., 16 h (13%); (ix) DIBAL-H (1M in PhMe), PhME, -20 °C to 0 °C, 2 h (20%).

For the synthesis of **17** (**Scheme 7**), we envisaged a coupling between pyrrole-2-carboxylic acid and the bromide **85** to obtain the key intermediate **86**, which could then be coupled with *tert*-butyl 4-aminopiperidine-1-carboxylate to provide the protected intermediate **87**. For the preparation of **85**, we started from the reduction of β-cyclocitral **54** to the hydroxyl intermediate **84** [40], which was then treated with PBr₃ to obtain the bromide **85** [41]. The latter proved to be unstable, and for this reason it was not purified but immediately used for the next coupling reaction with pyrrole-2-carboxylic acid. According to a previously procedure [42], this coupling can be performed in the presence of caesium carbonate, with the bromide reacting not only with the imidazole, but also with the carboxylic acid moiety. Consequently, a further saponification reaction could be necessary to restore the desired carboxylic acid group in **86** [42]. However, only the direct formation of the desired product **86** was observed in our hands. For the next coupling reaction with Boc-protected 4-aminopiperidine to obtain **87**, different attempts were performed. The use of two different coupling reagents (CDI and TBTU) was explored to convert the carboxylic acid group into a more reactive species, so that the amide bond formation could be accomplished. Although the reactions were refluxed for 24 h, in both cases only the two starting materials were recovered. The approach for the carboxylic acid activation was therefore changed: instead of using a coupling reagent, we envisaged the conversion of the carboxylic acid group into a more reactive acyl chloride in **88**.

Accordingly, **86** was reacted with oxalyl chloride in DCM with a catalytic amount of DMF to form the acyl chloride **88** [43], which was not isolated but directly treated with the Boc-protected 4-aminopiperidine in the presence of Et₃N as a base [43]. However, although the amide bond formation was achieved, the reaction conditions caused the dealkylation of the imidazole moiety and compound **89** was the main species isolated from the reaction mixture with a 48% yield. The successful coupling reaction conditions employed for **86** were therefore applied to react alkyl bromide **85** with **89**, to finally yield Boc-protected intermediate **90**, which needed to be deprotected to insert the aldehyde function of the final target product **17**. However, a useful methodology for the preparation of formamide derivatives from amines and formic acid in the presence of the cheap and non-toxic thiamine hydrochloride catalyst was applied [44], which allowed for the *in situ* deprotection of the piperidine nitrogen thanks to the excess of formic acid used, and enabled the isolation of the final product **17**.
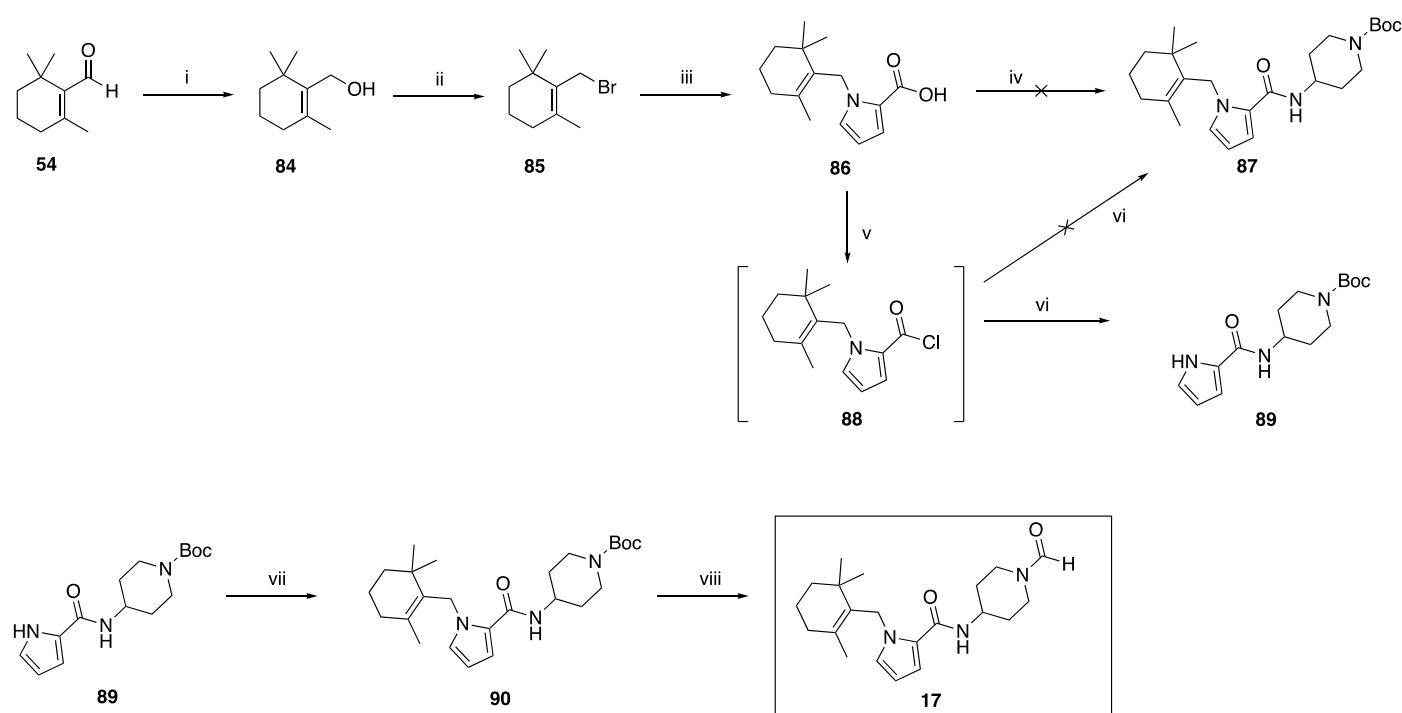
Scheme 7. Synthesis of target compound **17**. *Reagents and conditions*: (i) NaBH₄, *i*PrOH, EtOH, 0 °C to r.t., 3 h (quant.); (ii) PBr₃, hexane, Et₂O, -20 °C, 15 min. (89%); (iii) pyrrole-2-carboxylic acid, Cs₂CO₃, DMF, r.t., 16 h (92%); (iv) *tert*-butyl 4-aminopiperidine-1-carboxylate, CDI or TBTU, DMF, reflux, 16 h (traces); (v) (COCl)₂, car. DMF, 0 °C to r.t., 3 h; (vi) *tert*-butyl 4-aminopiperidine-1-carboxylate, Et₃N, CH₂Cl₂, 0 °C to r.t., 16 h (48%); (vii) **85**, Cs₂CO₃, DMF, r.t., 16 h (34%) ; (viii) HCOOH, thiamine HCl, 120 °C in a sealed tube, 16 h (20%).

Finally, the synthetic preparation of **18** began with a coupling reaction between the deprotected piperidone **92** and the carboxylic acid derivative of β-ionone **50** (**Scheme 8**). The carboxylic acid group was activated using TBTU as coupling reagent to enable attack from piperidone **92**, with the formation of an amide bond in **93**. To accomplish the synthesis of the α,β-unsaturated carboxylic acid **18**, **93** was reacted with triethyl phosphonoacetate in the presence of NaH. According to a previously reported procedure [45], formation of the ester derivative **94** was expected, but instead the target final compound **18** was the only product detected and isolated in this reaction. Different attempts were made to reduce the acid function to aldehyde and obtain also the aldehyde analogue **95**, using either DIBAL-H or LiALH₄, but both these reactions failed and only traces of **95** were observed.
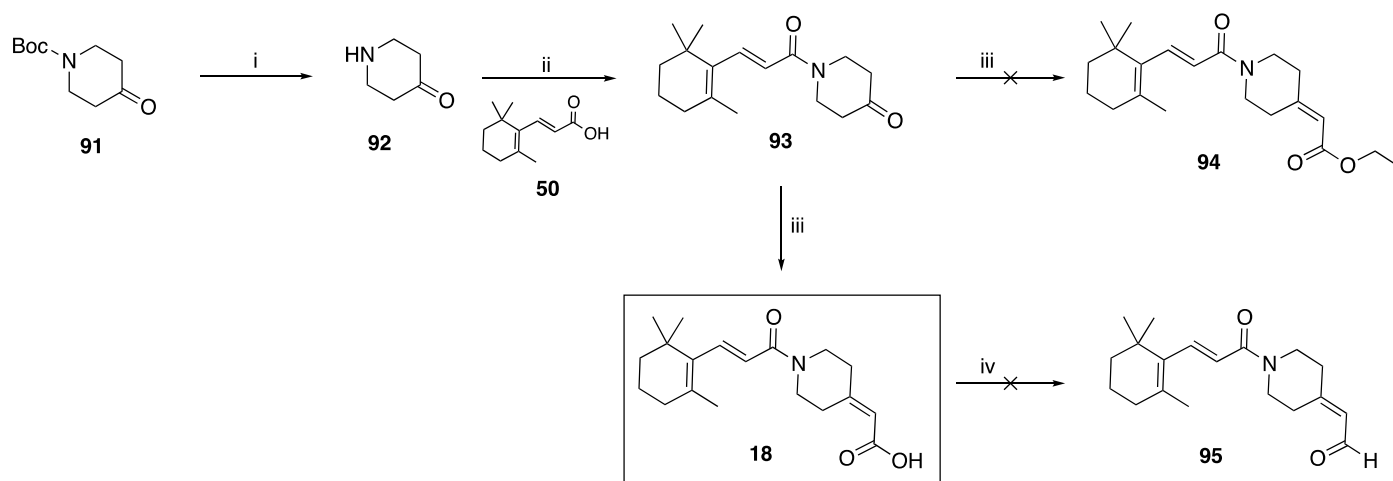
Scheme 8. Synthesis of target compound **18**. *Reagents and conditions*: (i) b) TFA/CH$_2$Cl$_2$ (1:1, v/v), 0 °C to r.t., 3 h (quant.); (ii) TBTU, DIPEA DMF, 0 °C to r.t., 2 h (64%); (iii) NaH (60% oil dispersion), triethyl phosphonoacatate, THF, r.t., 16h (17%); (iv) DIBAL-H (1 M in PhMe), PhMe, -78 °C to 0 °C, 1h (traces).

2.3. Biological assays

The novel target compounds prepared were evaluated for their potential to act as chemical chaperones for opsin in both a competitive binding assay and an immunofluorescence assay to monitor the cellular trafficking of the P23H opsin mutant.

2.3.1 Competitive binding assay

The new molecules **1-14** were evaluated for their potential ability to bind rhodopsin by monitoring the generation rate of bovine isorhodopsin through time-dependent UV-VIS spectroscopy. In this assay, rhodopsin is added of 9-*cis*-retinal, which is a chromophore with photoactivation similar to 11-*cis*-retinal, but more stable, resulting in a time-dependent increase in optical density at 485 nm [3, 15, 46]. Compounds that compete with 9-*cis*-retinal for the binding to rhodopsin reduce the rate constant (k) of the formation of the rhodopsin-9-*cis*-retinal complex. The compounds were pre-incubated for 30 min with freshly bleached rhodopsin followed by addition of 9-*cis*-retinal (**Materials and Methods**). The rate constant k of the complex regeneration was calculated and compared to mock pre-incubated samples with vehicle only (DMSO, k = 0.50 ± 0.03 min^{-1}, t$_{1/2}$= 1.43 ± 0.09 min, Mean ± SEM). β-ionone, CF35EsC and CF35Es were used as positive controls. CF35EsC and CF35Es were synthesised as previously reported [15]. β-Ionone significantly reduced the regeneration kinetic (k = 0.20 ± 0.01 min^{-1}, t$_{1/2}$= 3.60 ± 0.18 min), confirming its ability to occupy the chromophore binding site (**Figure 9**, **Table S1**), as previously observed [15].
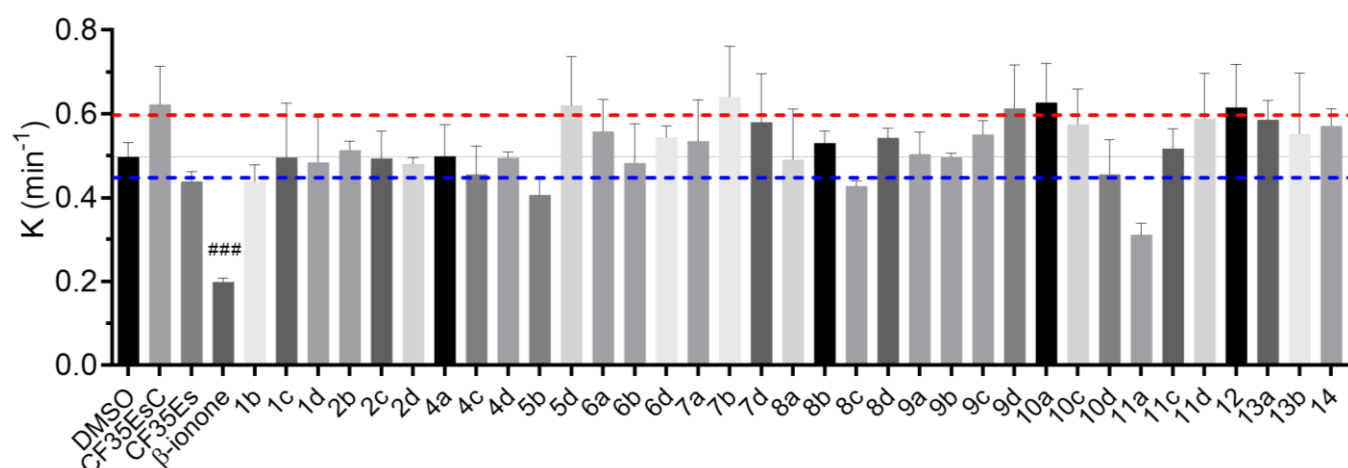
Figure 9. Effect of compounds **1-14** (compound concentration ~10 times 9-*cis*-retinal) on the rate constant (**k**) of bovine isorhodopsin generation (see *Supporting Information* (**Table S1**) for details). After rhodopsin bleaching with green light of 532 nm wavelength, compounds were pre-incubated for 30 min followed by addition of 9-*cis*-retinal and recording of absorbance at 485 nm for 30 min. β-ionone, CF35EsC and CF35Es were used as positive controls. Compounds were considered as hits when k ≥ 10% decreased (blue dashed line) or ≥ 20% increased (red dashed line) compared to DMSO (vehicle). Error bars represent mean ± SEM of pooled data (at least three independent measurements). Data were analysed using one-way ANOVA, followed by Fisher's LSD test versus DMSO controlled for false discovery rate (FDR) by the two-stage step-up method of Benjamini, Krieger and Yekutieli . # = discovery with *q* < 0.05.

The positive controls CF35EsC and CF35Es have been reported to induce proper trafficking of P23H rhodopsin from the ER to the cell-surface [14], and we had previously observed that CF35Es competes for the occupation of the chromophore site (10% decrease of k value; k = 0.44 ± 0.02 min^{-1} compared to DMSO), while CF35EsC instead increases the k value by over 20% (k = 0.62 ± 0.09 min^{-1}) [15]. Based on this, we had speculated that CF35EsC may act as an allosteric modulator of rhodopsin, possibly facilitating the retinal access to the binding site enhancing and speeding up the formation of the opsin-9-*cis*-retinal complex or stabilising the complex after its formation. This is in line with previous observations that β-ionone is an enhancer of the catalytic activity of different visual pigments, in which the chromophore binding site was already occupied, possibly acting as an allosteric modulator [47-48]. A series of flavonoid compounds have also been proposed as allosteric modulators able to enhance opsin stability by modulating its conformation [49], and we had previously suggested a similar effect for CF35EsC, which could still occupy opsin orthosteric pocket, but its ability of facilitating/stabilising the rhodopsin-9-*cis*-retinal complex formation appears to be the dominant effect [15]. Stabilisation of rhodopsin and preventing its degradation, either in the absence of 11-*cis*-retinal (LCA) or in the presence of aberrant mutations (RP), could provide an alternative therapeutic mechanism to the chaperone action carried out by direct occupation of the orthosteric pocket. Of the 35 novel molecules tested in this assay, three compounds, namely **5b**, **5c** and **11a**, exhibited a promising decrease by 10% (or more) of the rate constant k compared to vehicle control (**5b**: k = 0.41 ± 0.04 min^{-1}; **8c**: k = 0.43 ± 0.01 min^{-1}; **11a**: **k** = 0.31 ± 0.03 min^{-1}), showing the ability to bind the chromophore orthosteric pocket and compete with 9-*cis*-retinal. In particular, **11a** has the best activity profile, reducing k by 37%. Kinetics of isorhodopsin generation in the presence of DMSO and **11a** are reported in the *Supporting Information* (Figure S1). In addition, six molecules, **5d**, **7b**, **9d**, **10a**, **11d** and **12** (**5d**: k = 0.62 ± 0.11 min^{-1}; **7b**: k = 0.64 ± 0.12 min^{-1}; **9d**: **k** = 0.61 ± 0.10 min^{-1}; **10a**: **k** = 0.63 ± 0.09 min^{-1}; **11d**: **k** = 0.59 ± 0.10 min^{-1}; **12**: k= 0.62 ± 0.10 min^{-1}) show the same behaviour observed for CF35EsC, as they increase the k value by ~20% or over, potentially possessing the ability to stabilize and enhance the opsin-9-*cis*-retinal complex formation.

A trend in this activity profile is difficult to identify, as the hit molecules in this assay belong to different structural families, with the only exceptions of compounds **5b** (decreased k) and **5d** (increased k), and **11a** (decreased k) and **11d** (increased k). However, these results indicate that different compounds with therapeutic potential for RP and LCA fall into two distinct categories: molecules that compete for the binding to the orthosteric pocket (decreased k), which may act as chemical chaperones, and molecules that facilitate formation of/stabilise the opsin-9-*cis*-retinal complex (increased k), which may act as allosteric stabilisers. Interestingly, for scaffolds **5** and **11**, which both have one analogue decreasing k (**5b** and **11a**), and one analogue increasing k (**5d** and **11d**), the carboxamide derivative (**5d** and **11d**) is associated with the potential allosteric stabilising effect, possibly due to a weaker direct interaction with Lys296 in comparison with an aldehyde function (**5b**) and a nitrile group (**11a**), which could both form a transient covalent bond with Lys296. This trend however cannot be extended to the other hit scaffolds identified, as **7b** (aldehyde) and **10a** (nitrile analogue) both increase k, despite the potential to form a covalent bond with Lys296. Nonetheless, this stronger interaction with Lys296 could depend on an optimal orientation of the reactive functional group in the binding pocket, which may be achieved selectively with some of the new structural scaffolds, and not with others.

2.3.2 Immunofluorescence microscopy

The novel compounds **1-16**, along with **73** and **75**, were evaluated for their ability to induce the physiological trafficking of the P23H rhodopsin mutant in a cell-based experiment (U2OS cell line stably expressing P23H human rhodopsin), in order to assess their pharmacologic potential to rescue rhodopsin. As previously described [15], this immunostaining assay evaluated the localization of P23H human rhodopsin tagged with 6x Histidines at the C-terminus (hRHO P23H His-Tag) by detecting rhodopsin trafficked to the cell membrane using an anti-rhodopsin antibody (RetP1, binding to an N-terminus epitope, extracellular) under non-permeabilised conditions. Fluorescence signal of RetP1 are shown in red in Figure 10-11. Following cell permeabilisation, the total expressed rhodopsin was then detected with an anti-His-tag antibody (fluorescence signal shown in green). The presence of a small tag (His-tag) at the C-terminus was

previously investigated and reported to minimally affect the correct trafficking of wild-type human rhodopsin in this assay [15]. In our experiments, P23H mutant rhodopsin failed to show proper trafficking and homogeneous cell surface distribution, however 9-*cis*-retinal substantially rescued trafficking to the cell surface (**Figure 10A**) [15]. Cells treated with the two standards CF35EsC and CF35Es also showed a mild improvement in P23H mutant opsin localisation on the membrane (**Figure 10B**). Results obtained in this assay for all our novel compounds **1-16** are listed in the *Supporting Information* (**Figure S2**). Unfortunately, no data could be obtained for novel analogues **3a**, **3b**, **4b**, **17** and **18**, due to solubility issues at the tested concentration. Among our novel target molecules, the best results in this assay can be observed for **11a**, which elicits a detectable increase in the trafficking of P23H mutant from the ER to the cell membrane (**Figure 10C**).
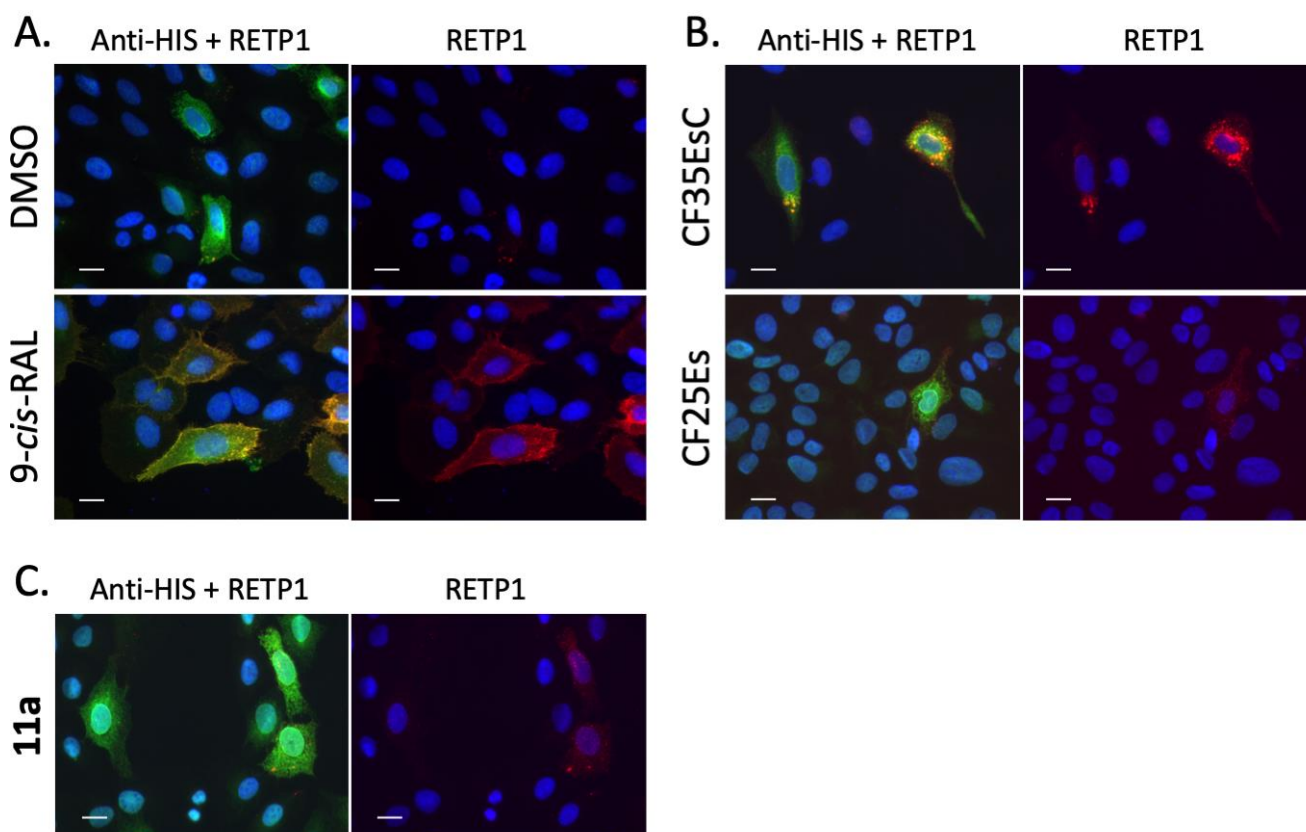
Figure 10. Subcellular localization of hRHO P23H His-Tag in presence of **9-cis-retinal** (**A**), **CF35EsC** and **CF35Es (B)** and **11a** (**C**) (representative images). **9-*cis*-Retinal** was tested at 5 μM, whereas **CF35EsC**, **CF35Es** and **11a** at 17 μM. DMSO did not exceed 0.1% final concentration. Anti-His/RetP1: merged images of cells stained with RetP1 antibody binding to the extracellular epitope of rhodopsin (red), and Anti-His Tag antibody binding total rhodopsin after membrane permeabilisation with 0.1% Triton (green). RetP1: anti-rhodopsin antibody fluorescence signal (red; incubation of RetP1 and subsequent AlexaFluor555 anti-mouse antibody was carried out prior to permeabilization). Nuclei were stained with DAPI (blue). Scale bars: 10 μm.

Additional compounds that show a similar effect to **11a**, although to a lesser extent, were **1c**, **2b**, **4c**, **5b**, **5d**, **6a**, **7b**, **10d-e**, **11c-d** and **13a-c** (**Figure 11**). For the remaining compounds, only reticular distribution consistent with ER retention was detected (*Supporting Information*, **Figure S2**). Although there does not appear to be a clear-cut correlation between the competitive binding assay and this cell-based experiment, **11a** is the best hit found in both assays, and it is likely to act as chemical chaperone for opsin, since it competes for binding to the chromophore orthosteric pocket. The same could potentially be assumed for **5b**, which also decreases k in the competitive binding assay. Compounds **5d**, **7b** and **11d** instead are likely to act as rhodopsin stabilisers by binding to a secondary site, as they are associated to an increased k value in the competitive binding assay. In both cases (compounds **11a** and **5b** versus **5d**, **7b** and **11d**), the correct folding of mutant P23H rhodopsin appears to be partially restored, as it allowed its proper trafficking of to the membrane. The activity observed for these compounds in both assays, especially for **11a**, can be considered a promising starting point for further development and investigations on their molecular scaffolds, which are currently ongoing.
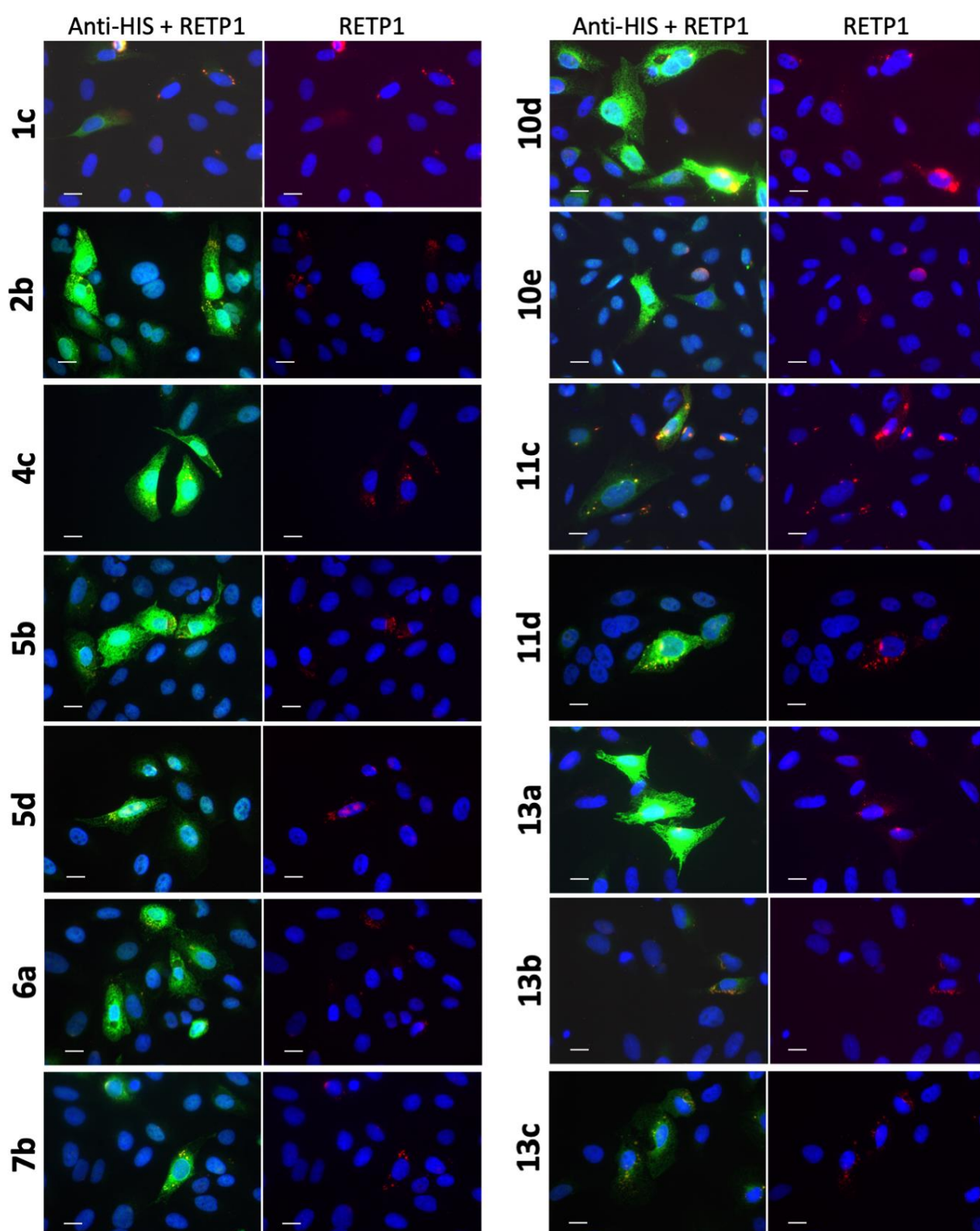
Figure 11. Subcellular localization of hRHO P23H His-Tag in the presence of novel target compounds **1c**, **2b**, **4c**, **5b**, **5d**, **6a**, **7b**, **10d, 10e, 11c, 11d** and **13a-c** (representative images). The compounds were tested at 17 μM or 20 μM (see *Supporting Information* (**Table S1**) for concentration tested corresponding to each compound). DMSO final concentration was 0.1%. Anti-His/RetP1: merged images of cells stained with RetP1 (red; binding an extracellular epitope of rhodopsin therefore rhodopsin trafficked to the membrane), and Anti-His Tag antibody (green; total rhodopsin, applied after membrane permeabilisation with 0.1% Triton). RetP1: anti-rhodopsin antibody fluorescence signal (red; staining with RetP1 and subsequent AlexaFluor555 anti-mouse antibody was performed prior to permeabilization). Nuclei were stained with DAPI (blue; post-permeabilisation). Scale bars: 10 μm.

2.3.3 Evaluation of cytotoxicity for selected hit compounds

The most interesting compounds identified in the two assays, along with the two positive controls CF35EsC and CF35Es and β-ionone, were evaluated for their potential cytotoxicity using the cell lines HepG2 and ARPE-19. HepG2 cells are widely used as an *in vitro* model for the detection of liver toxicity [50], while ARPE-19 cells are models for human retinal pigment epithelial cells. In the two assays, additional examples of the novel compounds were also included (**8d**, **6d**, **15**). Most compounds showed no significant toxic effect in both cell lines at the test concentration (**Figure 12**), with the only exception of **10a**, which reduced cell viability of HepG2 only by around 50%, and **11a**, which reduced cell viability of HepG2 only by around 25%. As **11a** is the best hit identified in this study, further structural modifications to its scaffold with the aim to improve its drug-like properties are the object of current research efforts.
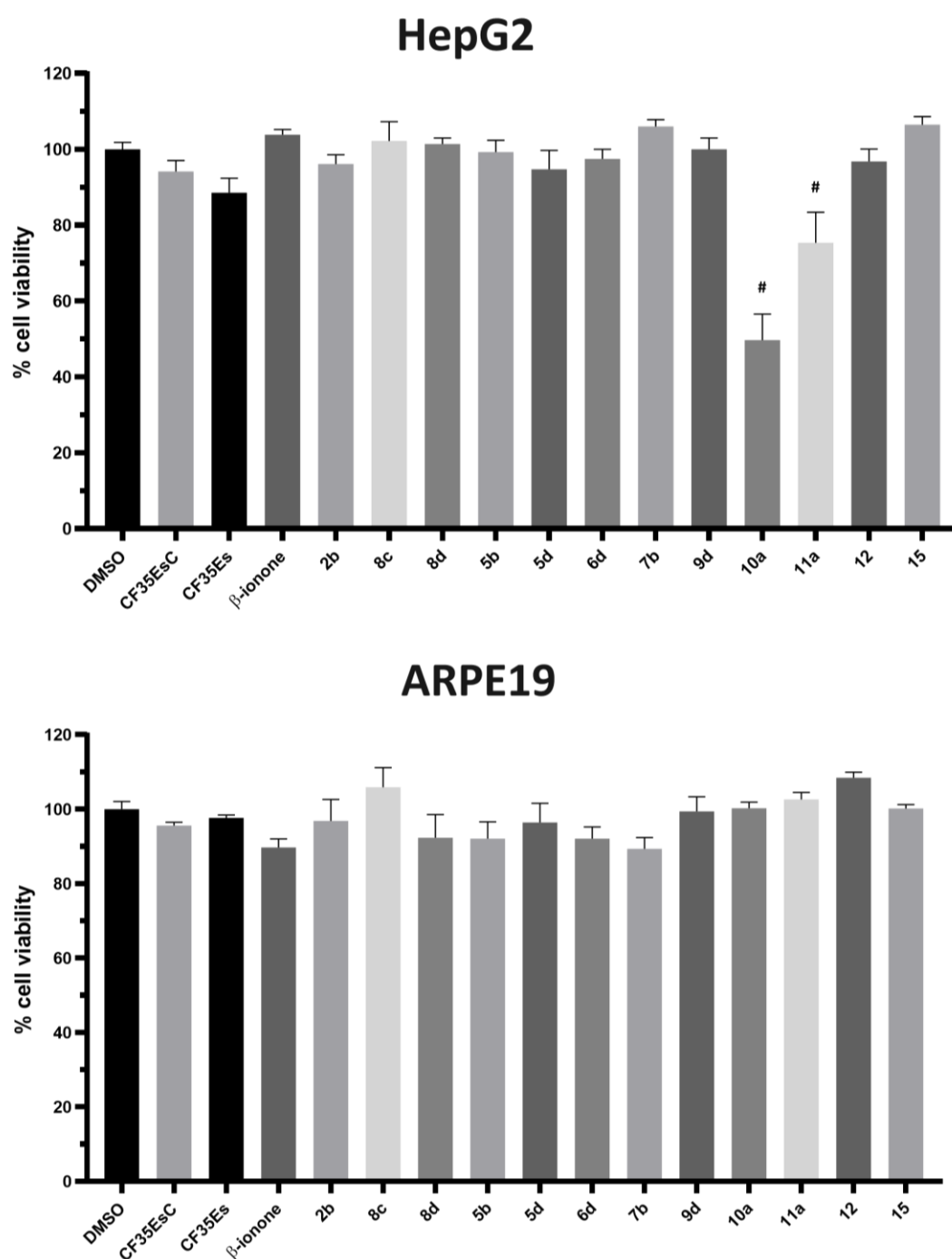
Figure 12. Potential cytotoxic effect for selected novel compounds on HepG2 and ARPE-19 cells. The concentration of all test compounds was 25 μM. The cell viability was determined as percentage of vehicle control-treated cells (DMSO). Bars represent mean ± SEM of at least three independent measurements. Data were analysed using one-way ANOVA, followed by Fisher's LSD test versus DMSO controlled for false discovery rate (FDR) by the two-stage step-up method of Benjamini, Krieger and Yekutieli. # = discovery with q < 0.05.

2.4. Molecular dynamics simulations

To further explore and confirm their ability to occupy opsin orthosteric pocket, as suggested by the molecular docking analyses, 100 ns molecular dynamics (MD) simulations were performed for compounds **11a** and **5b** in complex with opsin (PDB ID 1U19). All simulations were run in triplicate, using the Desmond software package [51]. As observed in our previously published work [15], the protein–ligand systems reach stability after an initial equilibration of 40-45 ns, converging around a fixed RMSD value, as shown by the small C-alpha RMSD variation (*Supporting Information*, **Figure S3**), which is then maintained for the remaining 60 ns of all the simulations. Both compounds optimized their occupancy of the 11-*cis*-retinal orthosteric site, maintaining a stable occupation during the entire simulation (**Figure 13** and *Supporting Information*, **Figure S4**). The compounds maintained respectively the nitrile (**11a**) and the aldehyde (**5b**) functional groups in close proximity to Lys296, while adjusting and orienting the remaining part of their molecular scaffolds towards the hydrophobic portion of the binding site, establishing different hydrophobic contacts with the surrounding residues (i.e., Met207, Phe208, Phe212 Trp265, and Ala272). **11a** is further stabilized in the binding pocket by the formation of an electrostatic interaction between its aromatic amine group and the sidechain carboxylate of Glu122, possibly explaining its higher potency compared to **5b** in both the assays performed. These findings further support the identified ability of these two active analogues to compete for the chromophore binding pocket in the competitive binding assay, and to produce the desired effect of inducing opsin trafficking to the outer cell membrane observed in the cell-based assay.
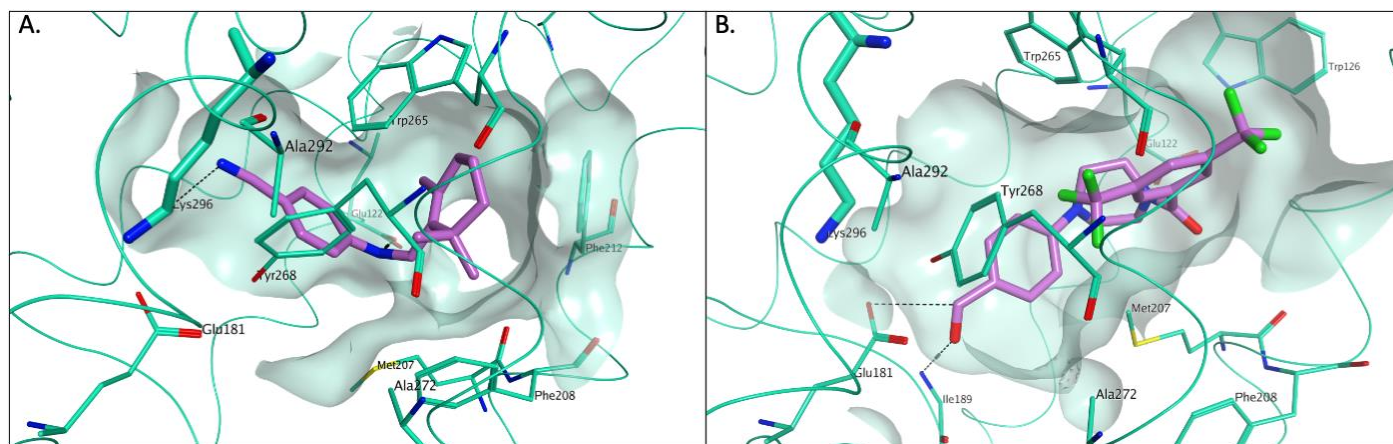
Figure 13. Binding mode for **11a** (A) and **5b** (B), carbon atoms in lilac, to ground-state rhodopsin (PDB ID 1U19) after MD simulation. The nitrile group and the aldehyde moiety of the two compounds, respectively, are placed nearby Lys296 during the entire simulation. The binding site area is represented as molecular surface. Rhodopsin is represented as green ribbon, with carbon atoms in green.

4. Conclusions

In this work, different novel small-molecule structural scaffolds were rationally designed as potential ligands of the main chromophore binding site of rhodopsin, to act as chemical chaperones for this protein in severe blinding conditions caused by its misfolding and mistrafficking. The effect of such compounds represents an attractive approach to slow down photoreceptor cell death and vision loss in patients affected by RP and LCA. 49 novel small molecules were successfully synthesized according to optimized synthetic routes. Except for those with significant solubility issues at the test concentrations, all the new compounds were evaluated for their ability to compete with 9-*cis*-retinal for binding to rhodopsin, monitoring the regeneration rate of bovine isorhodopsin through time-dependent UV-VIS spectroscopy. Three novel candidates showed a promising ability to reduce the rate constant (k) for the formation of the 9-cis-retinal-

opsin complex by 10-37%, acting as potential chemical chaperones for opsin. Six new molecules were found instead to facilitate the formation of/stabilise the opsin-9-*cis*-retinal complex by increasing the rate constant, revealing their potential to act as stabilizers of the protein folded structure. The novel compounds were also evaluated for their ability to induce the correct folding of mutant P23H rhodopsin, allowing its proper trafficking to the membrane in a fluorescent immunohistochemistry cell-based assay. This screening revealed different novel molecules with a promising effect of trafficking induction of the P23H mutant rhodopsin. Most of the hits identified in these two assays did not show relevant cytotoxicity in two different human cell lines (HepG2 and ARPE-19). Overall, these findings represent a promising starting point for further investigations on the molecular scaffolds of the novel hits identified, which are likely to act either as chaperones or structural stabilizers for rhodopsin, for the treatment of severe inherited eye diseases whose molecular basis is opsin misfolding and mistrafficking. Current structural optimization efforts are ongoing to improve the physical-chemical properties of these compounds, either to enhance their cell permeability, or to reduce any associated toxicity, which is a priority for the best candidate identified so far, compound **11a**.

5. Materials and Methods

5.1. Molecular docking studies

All molecular modelling experiments were performed on Asus WS X299 PRO Intel® i9-10980XE CPU @ 3.00GHz × 36 running Ubuntu 18.04 (graphic card: GeForce RTX 2080 Ti). Molecular Operating Environment (MOE) 2019.10 [52] and Maestro (Schrödinger Release 2020-2) [19] were used as molecular modelling software. The structures of the newly designed compounds were built in MOE, saved in .sdf format and prepared using the Maestro LigPrep tool by energy minimising the structures (OPLS_2005 force filed), generating possible ionization states at pH 7 ± 2, generating tautomers, generating all possible stereoisomers per ligand and low-energy ring conformers.

The crystal structure of bovine rhodopsin was downloaded from the PDB (http://www.rcsb.org/; PDB code 1U19). The protein was prepared using the MOE Protein Preparation tools, the bond between 11-cis-retinal and Arg296 (Schiff base) was disconnected and the resulting protein-ligand complex saved in .mae format to be used in Maestro for the docking simulations. The protein in .mae format was pre-processed using the Schrödinger Protein Preparation Wizard by assigning bond orders, adding hydrogens and performing a restrained energy minimisation of the added hydrogens using the OPLS_2005 force field. A 9 Å docking grid (inner-box 10 Å and outer-box 19 Å) was prepared using as centroid the co-crystallised 11-cis-retinal. The docking analyses were performed using Glide SP precision keeping the default parameters and setting as 25 the number of output poses per input ligand to include in the solution, performing for each pose a post-docking minimization. The docking results were then visually inspected using MOE 2019.10.

5.2. Synthetic chemistry

All solvents and reagents were used as obtained from commercial sources unless otherwise indicated. All solvents used for chromatography were HPLC grade from Fisher Scientific (UK). All reactions were performed under a nitrogen atmosphere. ^1H, ^{13}C and ^{19}F-NMR spectra were recorded with a Bruker Avance III HD spectrometer operating at 500 MHz for ^1H and 125 MHz for ^{13}C, with Me_4Si as internal standard. Deuterated chlo-roform was used as the solvent for NMR experiments, unless otherwise stated. ^1H chemical shifts values (δ) are referenced to the residual non-deuterated components of the NMR solvents (δ = 7.26 ppm for $CHCl_3$, etc.). The ^{13}C chemical shifts (δ) are referenced to $CDCl_3$ (central peak, δ = 77.0 ppm). TLC was performed on silica gel 60 F254 plastic sheets. Flash column chromatography was performed using a Biotage Isolera One automated system. UPLC-MS analysis was conducted on a Waters UPLC system with both Diode Array detection and Electrospray (+'ve and −'ve ion) MS detection. The stationary phase was a Waters Acquity UPLC BEH C18 1.7 μm 2.1 50 mm column. The mobile phase was LC-MS grade H_2O containing 0.1% formic acid (A) and LC-MS grade MeCN containing 0.1% formic acid (B). Column temperature: 40 °C. Sample diluent: MeCN. Sample concentration: 1 μg/mL. Injection volume: 2 μL. Three alternative methods were used: Linear gradient standard method (A): 90% A (0.1 min), 90–0% A (2.5 min), 0% A (0.3 min), 90% A (0.1 min); flow rate 0.5 mL/min. Linear gradient standard method (B): 90% A (0.1 min), 90–0% A (2.1 min), 0% A (0.8 min), 90% A (0.1 min); flow rate 0.5 mL/min. Linear gradient standard method (C): 90% A (0.1 min), 90–0% A (1.5 min), 0% A (1.4 min), 90% A (0.1 min); flow rate 0.5 mL/min. All compounds tested in biological assays were > 95% pure. Purity of in-termediates was > 90%, unless otherwise stated. Preparation and characterization of all intermediates and final products are fully described in the *Supporting Information*.

5.3. Biological assays

5.3.1 Retina Outer Segments (ROS) isolation from bovine eyes

Bovine eyes were attained from a local abattoir and shipped on ice in light-protective containers. Isolation of ROS was performed under dim red light following a modified protocol from Papermaster [53] and reported in our prior study [15]. Briefly, excised retina was homogenised in sucrose buffer (1.14 M Sucrose, 1 M NaCl, 0.1 M MgCl$_2$, 1 M Tris-acetate in H$_2$O) and separated through density gradient via serial ultracentrifugation (at 4°C). Quantification of opsin in isolated ROS (in phosphate buffer, PBS) was calculated through a UV-Vis spectrophotometer (absorption coefficient $\varepsilon_{280\ nm}$ = 81200 M^{-1} cm^{-1} and $\varepsilon_{500\ nm}$ = 40600 M^{-1} cm^{-1}).

5.3.2 Competitive binding assay

As previously reported [15], ROS membranes containing opsin were diluted to a final concentration of ~20-25 µM opsin in PBS buffer containing 1% N-dodecyl-b-maltoside (DM). This mixture was then bleached with green light (532 nm) from a laser diode and pre-incubated with the compounds for 30 min at room temperature (see *Supporting Information* (**Table S1**) for concentration tested corresponding to each compound). After this pre-incubation, UV–visible spectra of the samples were recorded before addition of 9-*cis*-retinal (equimolar concentration of opsin) and, after addition, at the following time points: 0, 1 min, 2 min, 3 min, 4 min, 9 min, 14 min, 19 min, 24 min, 29 min. Compounds CF35EsC, CF35Es [14] and β-ionone were used as positive controls. At least three repeats were measured for each condition. The kinetics of isorhodopsin generation (at 485 nm) were fitted by a one-phase association equation and pseudo-first order rate constant (k) were calculated using GraphPad Prism 7.0 (Graphpad Software, La Jolla, CA, USA)).

5.3.3 Cell culture

Cells were cultured in DMEM (HepG2) or DMEM/F12 1:1 (ARPE-19 and U2OS), enriched with 10% Foetal Bovine Serum (Sigma Aldrich and Gibco) and grown in standard culture conditions (in the dark, 37 °C, 5% CO$_2$ and appropriate humidity). All media (Gibco and Pan Biotech) were supplemented with antibiotics (100 units/mL penicillin, 1 µg/mL streptomycin, (Gibco)) and Glutamax (Gibco) as 1% of volume in a mixed solution. U2OS cells stably expressing – in presence of tetracycline – P23H human rhodopsin tagged with 6 Histidines at the C-terminus (P23H hRHO His-Tag) have been previously generated and described [15]. ARPE-19, human RPE cell line was purchased from ATCC (CRL-2302), while HepG2 cell line was kindly provided by Prof. Karl Hoffmann's lab, IBERS, (Aberystwyth University).

5.3.4 Determination of cell viability assessed by CellTiter-Blue

CellTiter-Blue Cell Viability Assay (Promega) was used according to the manufacturer recommended protocol to measure compound impact on cell viability. Briefly, cells were seeded in 96-well plates (1 x 10^4 per well) in complete culture media (containing 1 g/l glucose, 1x penicillin/streptomycin, 1x Glutamax, 2% FBS). The following day, media was replaced with 100 µL fresh media (2% FBS, 1g/L glucose) containing 25 µM of tested compound. Cells were then incubated at 37°C for 24 hours prior to addition of 20 µL of CellTiter Blue reagent to each well. Plates were then further incubated for 4 h at 37 °C to allow the CellTiter Blue reagent to be metabolised into a fluorescence product by living cells. Finally, the fluorescence was measured using excitation/emission wavelengths of 560/590 nm. Data were normalized to vehicle control-treated cells (DMSO).

5.3.5 Immunofluorescence microscopy

Immunostaining was carried out as previously reported [15]. Briefly, U2OS cells bearing the P23H hRHO His-Tag construct were plated on 13 mm polylysine-treated round glass coverslips until adherence. Media was replaced with media containing 1 µg/ml tetracycline and 5 µM 9-*cis*-retinal or compound using the same concentration as in the competitive biding assay (see *Supporting Information* (**Table S1**) for concentration tested corresponding to each compound). DMSO did not exceed 0.1% and was used as vehicle control at the same concentration. **CF35EsC** and **CF35Es** were used as positive controls. Overnight incubation in the dark allowed the tetracycline-induced expression of rhodopsin. On the following day, under dim red light conditions, cells were fixed for with methanol-free 4% paraformaldehyde, prior to blocking for 1 hour with TBS blocking buffer (LICOR). Cells were then stained with RET-P1 antibody (Invitrogen, 1:500)

followed by anti-mouse IgG (H+L), F(ab')2 Fragment Alexa Fluor® 555 Conjugate (Cell Signalling Technologies, 1:1000, TBS buffer) (each for at least for 1 hour). Coverslips were then carefully washed and cell membrane were permeabilised with Triton 0.1% for 20 minutes. Cells were then further stained with Anti-His Tag (Abgen, 1:500, TBS buffer, overnight) followed by anti-mouse IgG (H+L), F(ab')2 Fragment Alexa Fluor® 488 Conjugate antibody (Cell Signalling Technologies, 1:1000, TBS buffer, 1 hour). Finally, nuclei were stained with DAPI before microscope slides preparation. Cells were imaged with an Olympus BX50 epifluorescence microscope (from 3 independent experiments). Gain and exposure times for 488 nm and 555 nm channels were maintained constant across all coverslips from the same experiment. Every experiment included DMSO and 9-cis-retinal as negative and positive controls, respectively. Images were then post-processed with ImageJ software: 405 nm channel contrast was enhanced for clarity (DAPI channel, nuclei). No manipulations were made to the channels relevant in the experiments (488 and 555 nm). RGB colours were assigned to the three channels (blue to 405 nm, green to 488 nm and red to 555 nm) and images were merged with the software in-built function.

5.4. Molecular Dynamics silumations

Molecular dynamics simulations were performed using the Desmond package for MD simulation, employing OPLS_2005 force field in the explicit solvent and the TIP3 water model. The initial coordinates for the MD simulation were taken from the best docking poses obtained for each single compound. A cubic water box was used for the solvation of the system, ensuring a buffer distance of approximately 10 Å between each box side and the complex atoms. The systems were neutralised adding 5 chlorine counter ions. The system was minimised and pre-equilibrated using the default relaxation routine implemented in Desmond. A 100 ns MD simulation was performed, during which the equation of motion was integrated using a 2 fs time step in the NPT ensemble, with a temperature (300 K) and pressure (1 atm) constant. All other parameters were set using the Desmond default values. Data were collected every 8.5 ps (energy) and every 33.3 ps (trajectory). Each simulation was performed in triplicate, every time using a random seed as a starting point. Visualisation of the protein–ligand complex and MD trajectory analyses were carried out using Maestro. RMSD, secondary structure and protein–ligand interactions analyses were performed using the Simulation Event Analysis tool and the Simulation Interaction Diagram of Desmond.

Supplementary Materials: The following are available online at xxx.

Author Contributions: Conceptualization, M.B. and M.R.; methodology, M.B., G.P., E.P., M.S., C.V. and M.R.; investigation, M.B., G.P., E.P., M.S., C.V. and M.R.; resources, M.B., M.R. and A.B.; data curation, M.B., G.P., E.P., M.S. and C.V.; writing—M.B., E.P. and G.P.; writing—review and editing, all authors; supervision, M.B.; project administration, M.B.; funding acquisition, M.B, M.R. and A.B. All authors have read and agreed to the published version of the manuscript.

Conflicts of Interest: The authors declare no conflict of interest.

References

1.   Kiser, P.D.; Palczewski, K. Pathways and disease-causing alterations in visual chromophore production for vertebrate vision. J. *Biol. Chem.* **2021**, *296*, 100072.
2.   Palczewski, K. G protein-coupled receptor rhodopsin. *Annu. Rev. Biochem.* **2006**, *75*, 743-767.
3.   Kiser, P.D.; Golczak, M.; Palczewski, K. Chemistry of the retinoid (visual) cycle. *Chem. Rev.* **2014**, *114*, 194-232.
4.   Orban, T.; Jastrzebska, B.; Palczewski, K. Structural approaches to understanding retinal proteins needed for vision. *Curr. Opin. Cell Biol.* **2014**, *27*, 32-43.
5.   Surguchev, A.; Surguchov, A. Conformational diseases: Looking into the eyes. *Brain Res. Bull.* **2010**, *81*, 12-24.
6.   Dias, M.F.; Joo, K.; Kemp, J.A.; Ligório Fialho, S.; da Silva Cunha, A.; Woo, S.J.; Kwon, Y.J. Molecular genetics and emerging therapies for retinitis pigmentosa: Basic research and clinical perspectives. *Progr. Retin. Eye Res.* **2018**, *63*, 107-131.

7.   Chacon-Camacho, O.F.; Zenteno, J.C. Review and update on the molecular basis of Leber congenital amaurosis. *World J. Clin. Cases*. **2015**, *3*, 112-124.

8.   den Hollander, A.I.; Roepman, R.; Koenekoop, R.K.; Cremers, F.P.M. Leber congenital amaurosis: genes, proteins and disease mechanisms. *Prog. Retin. Eye Res.* **2008**, *27*, 391-419.

9.   Zhang, S.X.; Sanders, E.; Fliesler, S.J.; Wang, J.J. Endoplasmic reticulum stress and the unfolded protein responses in retinal degeneration. *Exp. Eye Res*. **2014**, *125*, 30-40.

10.   Botto, C.; Rucli, M.; Tekinsoy, M.D.; Pulman, J.; Sahel, J.A.; Dalkara, D. Early and late stage gene therapy interventions for inherited retinal degenerations, *Progr. Retin. Eye Res*. **2021**, *In Press*, 100975.

11.   Noorwez, S.M.; Ostrov, D.A.; McDowell, J.H.; Krebs, M.P.; Kaushal, S. A high-throughput screening method for small-molecule pharmacologic chaperones of misfolded rhodopsin. *Investig. Ophthalmol. Vis. Sci.* **2008**, 49, 3224-3230.

12.   Kuksa, V.; Bartl, F.; Maeda, T.; Jang, G.F.; Ritter, E.; Heck, M.; Van Hooser, J.P.; Liang, Y.; Filipek, S.; Gelb, M.H.; Hofmann, K.P.; Palczewski, K. Biochemical and Physiological Properties of Rhodopsin Regenerated with 11-cis-6-Ring- and 7-Ring-retinals. *J. Biol. Chem.* **2002**, *277*, 42315-42324.

13.   Chen, Y.; Chen, Y.; Jastrzebska, B.; Golczak, M.; Gulati, S.; Tang, H.; Seibel, W.; Li, X.; Jin, H.; Han, Y.; Gao, S.; Zhang, J.; Liu, X.; Heidari-Torkabadi, H.; Stewart, P. L.; Harte, W. E.; Tochtrop, G. P.; Palczewski, K. A novel small molecule chaperone of rod opsin and its potential therapy for retinal degeneration. *Nature Comm.* **2018**, *9*, 1976.

14.   Ohgane, K.; Dodo, K.; Hashimoto, Y. Retinobenzaldehydes as proper-trafficking inducers of folding-defective P23H rhodopsin mutant responsible for retinitis pigmentosa. *Bioorg. Med. Chem.* **2010**, *18*, 7022-7028.

15.   Pasqualetto, G.; Schepelmann, M.; Varricchio, C.; Pileggi, E.; Khogali, C.; Morgan, S. R.; Boostrom, I.; Rozanowska, M.; Brancale, A.; Ferla, S.; Bassetto, M. Computational Studies towards the Identification of Novel Rhodopsin-Binding Compounds as Chemical Chaperones for Misfolded Opsins. *Molecules* **2020**, *25*, 4904.

16.   Matsumoto, H.; Yoshizawa, T. Existence of a β-ionone ring-binding site in the rhodopsin molecule. *Nature* **1975**, *258*, 523-526.

17.   Daemen, F.J.M. The chromophore binding space of opsin. *Nature* **1978**, *276*, 847-848.

18.   Makino, C. L.; Riley, C. K.; Looney, J.; Crouch, R. K.; Okada, T. Binding of more than one retinoid to visual opsins. *Biophys. J.* **2010**, *99*, 2366-2373.

19.   Schrödinger Release 2020-2: Glide, Schrödinger, LLC, New York, NY, 2020.

20.   Pettinger, J.; Jones, K.; Cheeseman, M.D. Lysine-Targeting Covalent Inhibitors. *Angew. Chem.* **2017**, *56*, 15200-15209.

21.   Hoyt, E.A.; Cal, P.M.S.D.; Oliveira, B.L.; Bernardes, J.G.L Contemporary approaches to site-selective protein modification. *Nat. Rev. Chem.* **2019**, *3*, 147–171.

22.   Jackson, P. A.; Widen, J. C.; Harki, D. A.; Brummond, K. M. Covalent Modifiers: A Chemical Perspective on the Reactivity of α,β-Unsaturated Carbonyls with Thiols via Hetero-Michael Addition Reactions. *J. Med. Chem.* **2017**, *60*, 839–885.

23.   Keeley, A.; Petri, L.; Ábrányi-Balogh, P.; Keserű, G. M. Covalent fragment libraries in drug discovery. *Drug Discov. Today* **2020**, *25*, 983-996.

24.   Byrne, P.A.; Gilheany, D.G. The modern interpretation of the Wittig reaction mechanism. *Chem. Soc. Rev.* **2013**, *42*, 6670-6696.

25.   Carpino, L.A.; Imazumi, H.; El-Faham, A.; Ferrer, F.J.; Zhang, C.; Lee, Y.; Foxman, B.M.; Henklein, P.; Hanay, C.; Mügge, C.; Wenschuh, H.; Klose, J.; Beyermann, M.; Bienert, M. The Uronium/Guanidinium Peptide Coupling Reagents: Finally the True Uronium Salts. *Angew. Chem. Int. Ed.* **2002**, *41*, 441-445.

26.   Zacuto, M. J. Synthesis of Acrylamides via the Doebner–Knoevenagel Condensation. *J. Org. Chem.* **2019**, *84*, 6465–6474.

27.   Heravi, M. M.; Kheilkordi, Z.; Zadsirjan, V.; Heydari, M.; Malmir, M. Buchwald-Hartwig reaction: An overview. *J. Organomet. Chem.* **2018**, *861*, 17-104.

28.   Bellina, F.; Carpita, A.; Rossi, R. Palladium Catalysts for the Suzuki Cross-Coupling Reaction: An Overview of Recent Advances. *Synthesis* **2004**, 15, 2419-2440.

29.   Brady, S.F.; Hirschmann, R.; Veber, D.F. Some Novel, Acid-Labile Amine Protecting Groups. *J. Org. Chem.* **1977**, 143-146.

30.   Abdel-Magid, A. F.; Carson, K. G.; Harris, B. D.; Maryanoff, C. A.; Shah, R. D. Reductive Amination of Aldehydes and Ketones with Sodium Triacetoxyborohydride. Studies on Direct and Indirect Reductive Amination Procedures1. *J. Org. Chem.* **1996**, *61*, 3849–3862.

31.   Shonberg, J.; Herenbrink, C. K.; López, L.; Christopoulos, A.; Scammells, P. J.; Capuano, B.; Lane, J. R A Structure–Activity Analysis of Biased Agonism at the Dopamine D2 Receptor. *J. Med. Chem.* **2013**, *56*, 9199–9221.

32.   Aganda, K. C. C.; Hong, B.; Lee, A. Aerobic α-Oxidation of N-Substituted Tetrahydroisoquinolines to Dihydroisoquinolones via Organo-Photocatalysis. *Adv. Synth. Catal.* **2019**, *361*, 1124–1129.

33.   Kumpaty, H. J.; Bhattacharyya, S. Efficient Synthesis of N-Alkyl Tetrahydroisoquinolines by Reductive Amination. *Synthesis (Stuttg).* **2005**, *2005*, 2205–2209.

34.   Ning, Y.; Fukuda, T.; Ikeda, H.; Otani, Y.; Kawahata, M.; Yamaguchi, K.; Ohwada, T. Revisiting Secondary Interactions in Neighboring Group Participation, Exemplified by Reactivity Changes of Iminylium Intermediates. *Org. Biomol. Chem.* **2017**, *15*, 1381–1392.

35.   Lapierre, J.-M.; Rotstein, D.; Sjogren, E. New Retinoids for the Treatment of Emphysema. WO 02/28810 A2, 2 October 2000.

36.   Demont, E. H.; Andrews, B. I.; Bit, R. A.; Campbell, C. A.; Cooke, J. W. B.; Deeks, N.; Desai, S.; Dowell, S. J.; Gaskin, P.; Gray, J. R. J.; et al. Discovery of a Selective S1P1 Receptor Agonist Efficacious at Low Oral Dose and Devoid of Effects on Heart Rate. *ACS Med. Chem. Lett*. **2011**, *2*, 444–449.

37.	Orcel, U.; Waser, J. One-Pot Three-Component Synthesis of Vicinal Diamines via In Situ Aminal Formation and Carboamina-tion. *Angew. Chemie* **2016**, *128*, 12881-12885.

38.	Gini, A.; Bamberger, J.; Luis-Barrera, J.; Zurro, M.; Mas-Ballesté, R.; Alemán, J.; Mancheño, O. Synthesis of 3-Benzazepines by Metal-Free Oxidative C-H Bond Functionalization-Ring Expansion Tandem Reaction. *Adv. Synth. Catal.* **2016**, *358*, 4049.

39.	Sternbach, D. D.; Ensinger, C. L. Synthesis of Polyquinanes. 3. The Total Synthesis of (.+-.)-Hirsutene: The Intramolecular Diels-Alder Approach. *J. Org. Chem.* **1990**, *55*, 2725–2736.

40.	Mazur, M.; Gładkowski, W.; Podkowik, M.; Bania, J.; Nawrot, J.; Białońska, A.; Wawrzeńczyk, C. Lactones 43. New Biologically Active Lactones: β -Cyclocitral Derivatives. *Pest Manag. Sci.* **2014**, *70*.

41.	Crombie, B. S.; Smith, C.; Varnavas, C. Z.; Wallace, T. W. A Conjugate Addition–Radical Cyclisation Approach to Sesquiter-pene-Phenol Natural Products. *J. Chem. Soc. Perkin Trans. 1* **2001**, 2, 206–215.

42.	N'Zemba, B.; Sauve, G.; Sevigny, G.; Yelle, J. Aromatic Derivatives with HIV Integrase Inhibitory Properties. WO 02/26697 A2.

43.	Bisht, R.; Hoque, M. E.; Chattopadhyay, B. Amide Effect in C-H Activation: L-Shaped Ligand for Meta Borylation of Aromatic Amides via Noncovalent Interaction. *Angew. Chemie Int. Ed.* **2018**, *57*, 15762.

44.	Lei, M.; Ma, L.; Hu, L. A Convenient One-Pot Synthesis of Formamide Derivatives Using Thiamine Hydrochloride as a Novel Catalyst. *Tetrahedron Lett.* **2010**, *51*, 4186–4188.

45.	Takaya, J.; Sasano, K.; Iwasawa, N. Efficient One-to-One Coupling of Easily Available 1,3-Dienes with Carbon Dioxide. *Org. Lett.* **2011**, *13*, 1698–1701.

46.	Palczewski, K. Retinoids for treatment of retinal diseases. *Trends Pharm. Sci.* **2010**, *31*, 284–295.

47.	Isayama, T.; England, S.M.; Crouch, R.K.; Zimmerman, A.L.; Makino, C.L. β-ionone activates and bleaches visual pigment in salamander photoreceptors. *Vis. Neurosci.* **2009**, 26, 67–274.

48.	Makino, C.L.; Riley, C.K.; Looney, J.; Crouch, R.K.; Okada, T. Binding of more than one retinoid to visual opsins. *Biophys. J.* **2010**, *99*, 2366-73.

49.	Ortega, J.T.; Parmar, T.; Jastrzebska, B. Flavonoids enhance rod opsin stability, folding, and self-association by directly binding to ligand-free opsin and modulating its conformation. *J. Biol. Chem.* **2019**, 294, 8101–8122.

50.	Ramirez, T.; Felline, A.; Comitato, A.; Di Salvo, M.T.; Raimondi, F.; Gulati, S.; Fanelli, F. Prediction of liver toxicity and mode of action using metabolomics in vitro in HepG2 cells. *Arch. Toxicol.* **2018**, *92*, 893–906.

51.	Maestro-Desmond Interoperability Tools, version 3.1.; Schrödinger: New York, NY, USA, 2020; Available online: https://www.schrodinger.com/maestro (accessed on 7 September 2021).

52.	Molecular Operating Environment (MOE 2019.10); Chemical Computing Group, Inc.: Montreal, QC, Canada. Available online: http://www.chemcomp.com (accessed on 28 July 2021).

53.	Papermaster, D.S. Preparation of retinal rod outer segments. *Methods Enzymol.* **1982**, *81*, 48–52.